



**HAL**  
open science

## Impact of stress on cardiac phenotypes in mice harboring an ankyrin-B disease variant

Michael J Wallace, Nipun Malhotra, Juan Ignacio Elio Mariángelo, Tyler L Stevens, Lindsay J Young, Steve Antwi-Boasiako, Danielle Abdallah, Sarah Sumie Takenaka, Omer Cavus, Nathaniel P Murphy, et al.

► **To cite this version:**

Michael J Wallace, Nipun Malhotra, Juan Ignacio Elio Mariángelo, Tyler L Stevens, Lindsay J Young, et al.. Impact of stress on cardiac phenotypes in mice harboring an ankyrin-B disease variant. *Journal of Biological Chemistry*, 2023, 299 (6), pp.104818. 10.1016/j.jbc.2023.104818 . hal-04271860

**HAL Id: hal-04271860**

**<https://hal.science/hal-04271860>**

Submitted on 6 Nov 2023

**HAL** is a multi-disciplinary open access archive for the deposit and dissemination of scientific research documents, whether they are published or not. The documents may come from teaching and research institutions in France or abroad, or from public or private research centers.

L'archive ouverte pluridisciplinaire **HAL**, est destinée au dépôt et à la diffusion de documents scientifiques de niveau recherche, publiés ou non, émanant des établissements d'enseignement et de recherche français ou étrangers, des laboratoires publics ou privés.

1  
2  
3  
4 **Impact of stress on cardiac phenotypes in mice harboring an ankyrin-B**  
5  
6 **disease variant**  
7  
8  
9

10  
11 Michael J. Wallace<sup>1,2</sup>, Nipun Malhotra<sup>1,3</sup>, Juan Ignacio Elio Mariángelo<sup>1,2</sup>, Tyler L.  
12 Stevens<sup>1,2</sup>, Lindsay J. Young<sup>1</sup>, Steve Antwi-Boasiako<sup>1</sup>, Danielle Abdallah<sup>1</sup>, Sarah  
13 Sumie Takenaka<sup>1</sup>, Omer Cavus<sup>1</sup>, Nathaniel P. Murphy<sup>1</sup>, Mei Han<sup>1</sup>, Xianyao Xu<sup>1</sup>,  
14 Matteo E. Mangoni<sup>4</sup>, Thomas J. Hund<sup>1,5,6</sup>, Jason D. Roberts<sup>7</sup>, Sandor Györke<sup>1,2</sup>,  
15 Peter J. Mohler<sup>1,2,6</sup> and Mona El Refaey<sup>1,3\*</sup>  
16  
17  
18  
19  
20  
21  
22  
23  
24  
25

26 <sup>1</sup>The Frick Center for Heart Failure and Arrhythmia, Dorothy M. Davis Heart and Lung  
27 Research Institute, <sup>2</sup>Department of Physiology and Cell Biology, <sup>3</sup>Department of  
28 Surgery/Division of Cardiac Surgery, The Ohio State University, Columbus, OH, USA.  
29  
30

31 <sup>4</sup>Institut de Génomique Fonctionnelle, Université de Montpellier, CNRS, INSERM,  
32 Montpellier, France.  
33  
34  
35

36 <sup>5</sup>Department of Biomedical Engineering, College of Engineering, The Ohio State  
37 University, Columbus, Ohio, USA.  
38  
39  
40

41 <sup>6</sup>Department of Internal Medicine/Division of Cardiovascular Medicine, The Ohio  
42 State University, Columbus, OH, USA.  
43  
44  
45

46 <sup>7</sup>Population Health Research Institute, McMaster University, and Hamilton Health  
47 Sciences, Hamilton, Ontario, Canada.  
48  
49  
50  
51  
52  
53  
54  
55  
56

57 **Running Title: Impact of stress on the phenotype of ankyrin-B syndrome**  
58  
59  
60  
61  
62  
63  
64  
65

1  
2  
3  
4  
5  
6  
7  
8  
9  
10  
11  
12  
13  
14  
15  
16  
17  
18  
19  
20  
21  
22  
23  
24  
25  
26  
27  
28  
29  
30  
31  
32  
33  
34  
35  
36  
37  
38  
39  
40  
41  
42  
43  
44  
45  
46  
47  
48  
49  
50  
51  
52  
53  
54  
55  
56  
57  
58  
59  
60  
61  
62  
63  
64  
65

**\*Address correspondence to**

Mona El Refaey, PhD, MS

Department of Surgery/Division of Cardiac Surgery

The Dorothy M. Davis Heart and Lung Research Institute

The Ohio State University College of Medicine and Wexner Medical Center

333 West 10<sup>th</sup> Avenue, Columbus, OH, 43210

[Mona.elrefaey@osumc.edu](mailto:Mona.elrefaey@osumc.edu)

Tel: 614-366-2748

**Keywords:** ankyrin-B, bradycardia, incomplete penetrance, heart rate variability, fibrosis, arrhythmia, variant, heart failure, stress, cardiovascular disease.

Total word count of the manuscript: 9453

1  
2  
3  
4 **Abstract**  
5  
6

7  
8 Encoded by *ANK2*, ankyrin-B (AnkB) is a multi-functional adaptor protein  
9  
10 critical for the expression and targeting of key cardiac ion channels, transporters,  
11  
12 cytoskeletal-associated proteins, and signaling molecules. Mice deficient for AnkB  
13  
14 expression are neonatal lethal and mice heterozygous for AnkB expression display  
15  
16 cardiac structural and electrical phenotypes. Human *ANK2* loss-of-function variants  
17  
18 are associated with diverse cardiac manifestations, however human clinical ‘ankyrin-  
19  
20 B syndrome’ displays incomplete penetrance. To date, animal models for human  
21  
22 arrhythmias have generally been knock-out or transgenic overexpression models and  
23  
24 thus the direct impact of *ANK2* variants on cardiac structure and function *in vivo* is  
25  
26 not clearly defined. Here, we directly tested the relationship of a single human *ANK2*  
27  
28 disease-associated variant with cardiac phenotypes utilizing a novel *in vivo* animal  
29  
30 model. At baseline, young AnkBp.E1458G<sup>+/+</sup> mice lacked significant structural or  
31  
32 electrical abnormalities. However, aged AnkBp.E1458G<sup>+/+</sup> mice displayed both  
33  
34 electrical and structural phenotypes at baseline including bradycardia and aberrant  
35  
36 heart rate variability, structural remodeling, and fibrosis. Young and old  
37  
38 AnkBp.E1458G<sup>+/+</sup> mice displayed ventricular arrhythmias following acute  
39  
40 (adrenergic) stress. In addition, young AnkBp.E1458G<sup>+/+</sup> mice displayed structural  
41  
42 remodeling following chronic (transverse aortic constriction) stress. Finally,  
43  
44 AnkBp.E1458G<sup>+/+</sup> myocytes harbored alterations in expression and/or localization of  
45  
46 key AnkB-associated partners, consistent with the underlying disease mechanism. In  
47  
48 summary, our findings illustrate the critical role of AnkB in *in vivo* cardiac function as  
49  
50 well as the impact of single ankyrin-B loss-of-function variants *in vivo*. However, our  
51  
52  
53  
54  
55  
56  
57  
58  
59  
60  
61  
62  
63  
64  
65

1  
2  
3  
4 findings illustrate the contribution, and in fact necessity of secondary factors (aging,  
5  
6  
7 adrenergic challenge, pressure-overload) to phenotype penetrance and severity.  
8  
9

## 10 **Introduction**

11  
12  
13 Ankyrin-B (AnkB), encoded by *ANK2*, was first identified to play a role in the  
14  
15 nervous system via maintenance of pre-myelinated axons (1), and subsequently  
16  
17 determined to impact cardiac function. AnkB regulates the expression and targeting  
18  
19 of key membrane, cytoskeletal, and regulatory proteins, including the Na<sup>+</sup>/Ca<sup>2+</sup>  
20  
21 exchanger (NCX), Na<sup>+</sup>/K<sup>+</sup>-ATPase (NKA), voltage-gated calcium channel (Ca<sub>v</sub>1.3),  
22  
23  
24 protein phosphatase 2 A (PP2A) and β-spectrin (2,3). *ANK2* encodes multiple  
25  
26 isoforms and is subject to transcriptional regulation (4).  
27  
28  
29

30  
31 AnkB dysfunction is associated with diverse human cardiac phenotypes,  
32  
33 including QT prolongation, arrhythmogenic cardiomyopathy (ACM), sinus node  
34  
35 dysfunction, and atrial fibrillation. Rare *ANK2* variants may also function as modifiers  
36  
37 of wall thickness in hypertrophic cardiomyopathy (5). The broad spectrum of AnkB  
38  
39 molecular partners in the heart likely accounts for the corresponding broad range of  
40  
41 cardiac phenotypes associated with *ANK2* dysfunction. The constellation of clinical  
42  
43 features observed with *ANK2* dysfunction has been termed 'ankyrin-B syndrome' (6-  
44  
45  
46  
47  
48 10).  
49

50  
51 The human AnkBp.Glu1458Gly variant is associated with arrhythmias and  
52  
53 structural remodeling (7). However, ankyrin-B syndrome displays incomplete  
54  
55 penetrance, suggesting that AnkB variants alone may not be sufficient to directly  
56  
57 cause arrhythmia and/or structural phenotypes. Mouse gene knockout models may  
58  
59  
60  
61  
62  
63  
64  
65

1  
2  
3  
4 not replicate human molecular phenotypes (e.g. in case of dominant-negative  
5 variants). Therefore, we engineered a new animal model harboring the AnkB variant  
6 p.E1458G. Here, we illustrate two points: 1, single ankyrin-B variants are sufficient to  
7 cause cardiac phenotypes in six-month old AnkBp.E1458G<sup>+/+</sup> mice, and 2, acute  
8 and/or chronic stress augments the genesis of cardiac disease phenotypes in both  
9 young and old mice carrying the human variant. Our findings support a role of single  
10 *ANK2* variants in promoting mild cardiac phenotypes *in vivo*. However, severe *in vivo*  
11 phenotypes require secondary stressors including aging and adrenergic-stress.  
12  
13  
14  
15  
16  
17  
18  
19  
20  
21  
22  
23

## 24 **Results**

### 25 **Generation of a novel humanized knock-in mouse model**

26  
27  
28  
29  
30  
31 The AnkBp.E1458G variant (Figure 1A) is associated with ankyrin-B syndrome  
32 (3) and ACM (7). To test if this variant is sufficient to induce cardiac phenotypes *in*  
33 *vivo*, we generated a homozygous knock-in (KI) model (Figure 1B-C) harboring this  
34 single amino acid substitution. Cas9 was used to introduce a double strand  
35 chromosome break near codon 1371 in mouse (corresponds to 1458 in human  
36 sequence, ENSMUST00000182078.9). A single stranded oligonucleotide donor was  
37 used to change E1371 (E1458) to G1371 (G1458) and multiple silent coding changes  
38 were also introduced to block the Cas9 targets. Sanger sequencing chromatograms  
39 were used to confirm the substitution of glutamic acid (E) by glycine (G) in the KI  
40 mouse (Figure 1B-C). AnkBp.E1458G<sup>+/+</sup> mice were born at normal Mendelian ratios,  
41 29% control mice (40/137), 46% heterozygous mice (63/137) and 25% homozygous  
42 mice (34/137). *Ank2* mRNA expression levels were not changed in hearts of  
43 AnkBp.E1458G<sup>+/+</sup> mice compared to control littermates (Figure 1D). Canonical AnkB  
44  
45  
46  
47  
48  
49  
50  
51  
52  
53  
54  
55  
56  
57  
58  
59  
60  
61  
62  
63  
64  
65

1  
2  
3  
4 protein levels were not significantly different between AnkBp.E1458G<sup>+/+</sup> and control  
5  
6 littermate hearts (Figure 1E and F).  
7  
8

### 9 **Young AnkBp.E1458G<sup>+/+</sup> mice do not display cardiac phenotypes**

10  
11  
12 Three-month old AnkBp.E1458G<sup>+/+</sup> homozygous mice did not display structural  
13 phenotypes. Specifically, three-month old AnkBp.E1458G<sup>+/+</sup> mice did not display  
14 changes in ejection fraction or fractional shortening (Figure 2A, Suppl. Figure 1A, G  
15 and H). Moreover, AnkBp.E1458G<sup>+/+</sup> mice did not exhibit electrocardiogram  
16 alterations or arrhythmia phenotypes at three months of age (Suppl. Figure 2).  
17  
18  
19  
20  
21  
22  
23  
24

### 25 **Aged AnkBp.E1458G<sup>+/+</sup> mice display structural remodeling and reduced 26 cardiac function**

27  
28  
29  
30  
31 AnkBp.E1458G<sup>+/+</sup> mice showed a significant reduction in ejection fraction and  
32 fractional shortening at ~six months of age (Figure 2B-D, Suppl. Figure 1B and Suppl.  
33 Table 1). Six-month old AnkBp.E1458G<sup>+/+</sup> mice also exhibited a trend towards an  
34 increased LVID ( $p=0.0694$ , Suppl. Figure 1C) and decreased LVPW during systole  
35 ( $p=0.0971$ , Suppl. Figure 1D) that did not reach statistical significance. No significant  
36 changes were noted in LVID or LVPW during diastole (Suppl. Figure 1E-F). While  
37  
38 *Ank2*-cKO mice showed left ventricular dilation and increased body weight relative to  
39 tibial length (7), these findings were not observed in the AnkBp.E1458G<sup>+/+</sup> mice in  
40 this study (Figure 2E-G). Notably, six-month old AnkBp.E1458G<sup>+/+</sup> mice showed  
41 widespread cardiac fibrosis at baseline compared with control mice (Figure 2F and  
42  
43  
44  
45  
46  
47  
48  
49  
50  
51  
52  
53  
54  
55  
56  
57  
58  
59  
60  
61  
62  
63  
64  
65

1  
2  
3  
4 stress. No significant changes were noted in the cardiac remodeling markers  
5  
6 including  $\beta$ -myosin heavy chain (*Myh7*), atrial natriuretic peptide (*Nppa*), brain  
7  
8 natriuretic peptide (*Nppb*), Collagen type I alpha 1 chain (*Col1a1*) and Tissue inhibitor  
9  
10 matrix metalloproteinase 1 (*Timp1*) in the AnkBp.E1458G<sup>+/+</sup> mice at ~ six months of  
11  
12 age (Suppl. Figure 3).  
13  
14

### 15 16 17 **Aged AnkBp.E1458G<sup>+/+</sup> mice exhibit electrical phenotypes** 18 19

20 Conscious six-month old AnkBp.E1458G<sup>+/+</sup> mice exhibited sinus bradycardia  
21  
22 at rest (mean HR is 658.7±15.2 bpm in control mice vs. 590.5±21.58 bpm in  
23  
24 AnkBp.E1458G<sup>+/+</sup> mice; Figure 3A and B; p=0.03). Accordingly, the RR interval was  
25  
26 significantly prolonged in the AnkBp.E1458G<sup>+/+</sup> mice compared to the control  
27  
28 littermates (mean RR =0.0919 ± 0.0024 s in control mice vs. mean RR in  
29  
30 AnkBp.E1458G<sup>+/+</sup> mice = 0.1035 ± 0.0040 s; Figure 3F; p=0.04). No significant  
31  
32 changes were noted in the P wave duration, PR interval or the QRS duration (Figure  
33  
34 3C-E and Suppl. Table 2). AnkBp.E1458G<sup>+/+</sup> mice showed a statistically significant  
35  
36 prolongation in the QT-interval (mean= 0.0206 ± 0.0007 s in control mice vs. mean=  
37  
38 0.0231 ± 0.0006 s, p=0.02). However, the corrected QT interval (Mitchell et al. (11))  
39  
40 trended toward prolongation in the AnkBp.E1458G<sup>+/+</sup> mice, but did not reach  
41  
42 statistical significance (mean= 0.0216 ± 0.0006 s in control mice vs. mean= 0.0228 ±  
43  
44 0.0007 s, p=0.25;Figure 3G and H). There is a debate on whether the QT interval is  
45  
46 affected by heart rate in small animals (12-14) and therefore, we measured both  
47  
48 intervals and displayed QTc according to Mitchell et al (11).  
49  
50  
51  
52  
53  
54  
55  
56

57 Abnormal high and low-frequency components of heart rate variability (HRV) may  
58  
59 suggest a dysfunction in autonomic regulation or an intrinsic sinus node dysfunction.  
60  
61  
62  
63  
64  
65

1  
2  
3  
4 Specifically, the high frequency (HF) component is modulated by the  
5  
6 parasympathetic nervous system, while the low frequency (LF) reflects the activity of  
7  
8 both parasympathetic and sympathetic nervous system (15). The high- and low-  
9  
10 frequency spectral components of HRV were significantly increased in the  
11  
12 AnkBp.E1458G<sup>+/+</sup> mice versus control littermates at rest (Figure 4A (p<0.01) and B  
13  
14 (p=0.02)) in line with mild bradycardia observed in AnkBp.E1458G<sup>+/+</sup> mice. Notably,  
15  
16 LF/HF ratio was significantly reduced in the AnkBp.E1458G<sup>+/+</sup> mice (Figure 4C  
17  
18 p=0.03). Analyzing the RR-interval of the control mice vs. the AnkBp.E1458G<sup>+/+</sup> mice  
19  
20 over a 14 min interval confirmed and displayed both prolongation and variability in  
21  
22 the aged mice harboring the single amino acid substitution, AnkBp.E1458G. Analysis  
23  
24 of RR and standard deviation of RR (SDRR) intervals displayed a significant increase  
25  
26 in both parameters in the AnkBp.E1458G<sup>+/+</sup> vs. the control mice (Figure 4D-E).  
27  
28 Representative traces from both genotypes over 1 min interval are displayed in  
29  
30 Figure 4F.  
31  
32  
33  
34  
35  
36  
37  
38

### 39 **AnkBp.E1458G<sup>+/+</sup> mice exhibit arrhythmia in response to adrenergic challenge**

40  
41  
42 Previous studies using *Ank2*-cKO mice noted polymorphic arrhythmia events  
43  
44 following adrenergic stimulation (7). Young mice harboring the human variant  
45  
46 displayed an increase in the number of ventricular arrhythmic events (control,  
47  
48 mean~0.7 events vs. AnkBp.E1458G<sup>+/+</sup> mice, mean ~18 events) (Figure 5A-D,  
49  
50 p=0.0325) when challenged with epinephrine. Moreover, six-month old mice also  
51  
52 showed a significant increase in the number of ventricular arrhythmia events  
53  
54 compared to their control littermates following epinephrine (control, mean ~14.5 ±  
55  
56 6.14 events and AnkBp.E1458G mice, mean ~35.8 ± 8.66 events) (Figure 6A,  
57  
58  
59  
60  
61  
62  
63  
64  
65

1  
2  
3  
4 p=0.04). Finally, when challenged with a stress protocol consisting of combined  
5  
6 epinephrine (2mg/kg) and caffeine (120mg/kg), the six-month old AnkBp.E1458G<sup>+/+</sup>  
7  
8 mice displayed a significant increase in the number of ventricular arrhythmic events  
9  
10 (control, mean ~18.3 ± 6.34 events and AnkBp.E1458G mice, mean ~116.8 ± 41.73  
11  
12 events) (Figure 6B, p=0.04). Notably, the number and duration of sustained episodes  
13  
14 of ventricular tachycardia (VT) were significantly higher and prolonged in the  
15  
16 AnkBp.E1458G<sup>+/+</sup> mice compared with control littermates (Figure 6C-D, p<0.01 and  
17  
18 p=0.03). The number of non-sustained ventricular tachycardia (NSVT) episodes  
19  
20 trended upward in AnkBp.E1458<sup>+/+</sup> mice (Figure 6E, p=0.14). Representative  
21  
22 recordings denoting episodes of VT and NSVT are included in (Figure 6F-H). Taken  
23  
24 together, AnkBp.E1458G<sup>+/+</sup> mice showed arrhythmic events following adrenergic  
25  
26 challenge or acute stressor at an early age. These events became more severe and  
27  
28 sustained in adult animals at six months of age.  
29  
30  
31  
32  
33  
34  
35

36  
37 Abnormal calcium handling may lead to cardiac electrical abnormalities either  
38  
39 through spontaneous calcium waves that cause delayed afterdepolarizations or  
40  
41 through calcium transient alternans, that provide a substrate for reentrant  
42  
43 mechanisms (16). In this study, we investigated calcium handling in cardiac myocytes  
44  
45 derived from AnkBp.E1458G<sup>+/+</sup> mice and control littermates in the presence (100 nM  
46  
47 and 500 nM) and absence of isoproterenol (ISO). As expected, ISO significantly  
48  
49 increased the amplitude and rate of decay of calcium transients (Figure 7A-C). We  
50  
51 observed that the amplitude and rate of decay of calcium transients were similar  
52  
53 between AnkBp.E1458G<sup>+/+</sup> and control myocytes ± ISO. Additionally, the frequency  
54  
55 of spontaneous calcium waves was comparable between the two groups (Figure 7D  
56  
57  
58  
59  
60  
61  
62  
63  
64  
65

1  
2  
3  
4 and E). Notably, AnkBp.E1458G<sup>+/+</sup> myocytes displayed a higher predisposition to  
5  
6 calcium transient alternans than WT myocytes (Figure 7F-H). In line with previous  
7  
8 studies (17,18), ISO tended to decrease the likelihood of alternans in WT myocytes.  
9  
10 However, in AnkBp.E1458G<sup>+/+</sup> myocytes, ISO increased the predisposition to  
11  
12 alternans (Figure 7G-H). Overall, these findings illustrate calcium handling  
13  
14 dysfunction in AnkBp.E1458G<sup>+/+</sup> myocytes.  
15  
16  
17  
18

### 19 **AnkBp.E1458G<sup>+/+</sup> mice develop severe cardiac phenotypes in response to** 20 **chronic cardiac pressure overload** 21 22 23 24

25 We hypothesized that young AnkBp.E1458G homozygous mice would develop  
26  
27 an accelerated structural phenotype in response to chronic cardiac stress. Therefore,  
28  
29 a model of pressure overload, transverse aortic constriction (TAC), was performed in  
30  
31 young AnkBp.E1458G<sup>+/+</sup> mice. AnkBp.E1458G<sup>+/+</sup> mice exhibited a significant  
32  
33 reduction in contractility or ejection fraction and fractional shortening at eight and  
34  
35 twelve weeks post TAC compared to control littermates (Figure 8A and B). Moreover,  
36  
37 AnkBp.E1458G<sup>+/+</sup> mice did not display significant differences in the LVID during  
38  
39 diastole or systole post TAC (Figure 8C-D). Furthermore, AnkBp.E1458G<sup>+/+</sup> hearts  
40  
41 displayed widespread cardiac fibrosis in the homozygous hearts post TAC (Figure  
42  
43 8E and F) compared with control mice. Comparing the relative expression of cardiac  
44  
45 remodeling markers between the young mice (~2-3months of age) and mice post  
46  
47 TAC, no significant changes were noted in *Myh7*. We observed a significant increase  
48  
49 in *Nppa* relative expression in the control and AnkBp.E1458G<sup>+/+</sup> hearts post TAC vs.  
50  
51 young control hearts (p=0.026 and p=0.025) and vs. young AnkBp.E1458G<sup>+/+</sup> hearts  
52  
53 (p=0.032 and p=0.0036). *Nppb* relative expression was upregulated in the  
54  
55  
56  
57  
58  
59  
60  
61  
62  
63  
64  
65

1  
2  
3  
4 AnkBp.E1458G<sup>+/+</sup> hearts post TAC compared to the young controls (p=0.0168) and  
5  
6 young AnkBp.E1458G<sup>+/+</sup> hearts (p=0.0125). *Col1a1* relative expression was  
7  
8 upregulated in the AnkBp.E1458G<sup>+/+</sup> hearts post TAC compared to the young  
9  
10 AnkBp.E1458G<sup>+/+</sup> (p=0.0467). Finally, *Timp1* was significantly upregulated in the  
11  
12 control (p=0.0382) and AnkBp.E1458G<sup>+/+</sup> (p=0.0199) hearts post TAC compared to  
13  
14 young AnkBp.E1458G<sup>+/+</sup> mice (Suppl. Figure 4).  
15  
16  
17  
18

19  
20 **Expression and localization of AnkB membrane partners is altered in**  
21  
22 **AnkBp.E1458G<sup>+/+</sup> hearts**  
23  
24

25 We investigated the expression of AnkB and AnkB-key binding partners,  
26  
27 including NCX and NKA, in our AnkBp.E1458G<sup>+/+</sup> mouse model at baseline, older  
28  
29 age and post TAC. Immunoblotting experiments showed no changes in the  
30  
31 normalized expression of AnkB in the AnkBp.E1458G<sup>+/+</sup> mice at six months of age  
32  
33 (Figure 9A and B). Additionally, *Ank2* mRNA levels were not different between the  
34  
35 two groups of mice at ~six months of age (Suppl. Figure 5). The expression of both  
36  
37 NCX and NKA was not different in the young AnkBp.E1458G<sup>+/+</sup> mice at ~2 months of  
38  
39 age (Suppl. Figure 6A-D). The expression of NCX was not different between the  
40  
41 groups (Figure 9C and D) at ~six months of age. However, NKA protein expression  
42  
43 normalized to GAPDH showed a significant decrease in the hearts of the aged  
44  
45 AnkBp.E1458G<sup>+/+</sup> mice (~30% reduction, p= 0.0023) (Figure 9E and F). Ankyrin-G  
46  
47 expression was unchanged between the two groups of mice (Figure 9G and Suppl.  
48  
49 Figure 7). Notably, NCX expression remained unchanged and the NKA expression  
50  
51 was significantly reduced in the AnkBp.E1458G<sup>+/+</sup> mice post TAC compared to the  
52  
53  
54  
55  
56  
57  
58  
59  
60  
61  
62  
63  
64  
65

1  
2  
3  
4 control mice (Suppl. Figure 6E-H). Finally, NKA protein was bound to the AnkB Ig in  
5  
6 the presence of the human variant (Suppl. Figure 8).  
7  
8

9  
10 AnkB is a cytoskeletal protein that anchors and regulates the organization and  
11  
12 localization of both NKA and NCX in a macromolecular complex. We observed no  
13  
14 significant changes in the localization of NKA and NCX in AnkBp.E1458G<sup>+/+</sup> isolated  
15  
16 myocytes in relation to ankyrin-B in young mice (Figure 10A-B, E-F). However,  
17  
18 immuno-labeling data in the aged AnkBp.E1458G<sup>+/+</sup> myocytes demonstrated a  
19  
20 reduction in NKA localization at the T-tubules (Figure 10C, G). NCX signal was  
21  
22 consistently similar in the aged AnkBp.E1458G<sup>+/+</sup> and control myocytes (Figure 10D,  
23  
24 H). In summary, six months old AnkBp.E1458G<sup>+/+</sup> myocytes display altered NKA  
25  
26 expression and localization.  
27  
28  
29  
30  
31

## 32 **Discussion**

33  
34  
35 The human AnkBp.E1458G variant was initially identified in a large French  
36  
37 family with a complex cardiac phenotype, including sinus node dysfunction,  
38  
39 ventricular arrhythmia, sudden cardiac death, and atrial fibrillation (6). This  
40  
41 phenotype, referred to as “AnkB-syndrome”, has been attributed to altered Ca<sup>2+</sup>  
42  
43 signaling when studied in a full-body haploinsufficient AnkB murine model (7,19). The  
44  
45 AnkBp.E1458G variant has also been implicated in other cardiac conditions, such as  
46  
47 ACM (5) and as a potential modifier of wall thickness in hypertrophic cardiomyopathy  
48  
49 (7). Notably, the same AnkBp.E1458G variant was identified by Hertz et al. in children  
50  
51 who suffered from sudden unexpected infant death (20,21). In summary, the range  
52  
53 of cardiac phenotypes identified to harbor the human AnkBp.E1458G variant are  
54  
55 diverse and complex.  
56  
57  
58  
59  
60  
61  
62  
63  
64  
65

1  
2  
3  
4 Despite numerous reports identifying the AnkBp.E1458G missense variant in  
5 cases of cardiac disease, the variant has also been identified in non-diseased  
6 populations, raising questions about its pathogenicity and penetrance (9,22).  
7 Interestingly, Ware and colleagues reported that 49 of 64 published *ANK2* variants  
8 were either “benign” or “probably benign” (23). AnkB plays a role in the transport and  
9 localization of numerous proteins to the membrane, transverse-tubule, and  
10 intercalated disc in cardiomyocytes. Although, the AnkBp.E1458G variant is not  
11 located where AnkB associates with key binding partners, the variant is localized  
12 close to the site critical for AnkB intramolecular association.  
13  
14  
15  
16  
17  
18  
19  
20  
21  
22  
23  
24  
25  
26

27 GnomAD data estimates the minor allele frequency of the AnkBp.E1458G AnkB  
28 variant to be 0.000535 ([https://gnomad.broadinstitute.org/variant/4-114269433-A-](https://gnomad.broadinstitute.org/variant/4-114269433-A-G?dataset=gnomad_r2_1)  
29 [G?dataset=gnomad\\_r2\\_1](https://gnomad.broadinstitute.org/variant/4-114269433-A-G?dataset=gnomad_r2_1)). Further, the AnkBp.E1458G variant is significantly more  
30 prevalent among individuals with European and Latin ancestry. Therefore, it is more  
31 frequent in the general population than the AnkB syndrome phenotype (24),  
32 consistent with the incomplete penetrance of the AnkB phenotype associated with  
33 the AnkBp.E1458G variant. These findings, coupled with the AnkBp.E1458G variant  
34 most often being identified in sporadic cases of cardiac disease without clear  
35 evidence of familial genotype-phenotype segregation, indicate that the variant must  
36 rely on additional genetic and/or environmental factors in order to manifest with a  
37 clinical phenotype.  
38  
39  
40  
41  
42  
43  
44  
45  
46  
47  
48  
49  
50  
51  
52  
53

54 The translational relevance of the haploinsufficient and knockout mice has  
55 previously been questioned given the strong mouse phenotype compared to the  
56 commonly mild human phenotype, coupled with *ANK2* variants implicated in human  
57  
58  
59  
60  
61  
62  
63  
64  
65

1  
2  
3  
4 disease most often being missense (25). Recently, developments in gene editing  
5  
6 technology have allowed us to study the specific AnkBp.E1458G variant in mice, that  
7  
8 may more effectively model the human phenotype. The newly developed KI murine  
9  
10 model homozygous for the AnkBp.E1458G variant (Figure 1) provides a new tool and  
11  
12 new insights into the pathogenesis and penetrance of the AnkB syndrome.  
13  
14

15  
16  
17 Notably, aged AnkBp.E1458G<sup>+/+</sup> mice displayed bradycardia (Figure 3) and  
18  
19 increased HF and LF spectral elements suggesting higher HR variability in mice at a  
20  
21 later age while the mice displayed a lower LF/HF ratio (Figure 4). Increase in HF and  
22  
23 LF is in line with lower basal heart rate observed in AnkBp.E1458G mice. The  
24  
25 increase in HRV seen in the KI mice might suggest an intrinsic sinus node dysfunction  
26  
27 associated with this variant that leads to increased heart variability as suggested by  
28  
29 a previous report (26). However, we cannot exclude that AnkBp.E1458G may also  
30  
31 present with increased activity of the parasympathetic nervous system. Additionally,  
32  
33 homozygous mice showed increased vulnerability to arrhythmic events in response  
34  
35 to adrenergic challenge as early as ~three months of age post adrenergic stimulation  
36  
37 (Figure 5). Aged mice showed propensity for more severe cardiac arrhythmic events,  
38  
39 more frequent events, and longer sustained runs of arrhythmic episodes in response  
40  
41 to adrenergic and caffeine administration (Figure 6). AnkBp.E1458G<sup>+/+</sup> myocytes  
42  
43 displayed a higher a predisposition to calcium transient alternans that provides a  
44  
45 potential substrate for reentrant mechanisms (Figure 7). TAC surgery, a model for  
46  
47 chronic cardiac stress, also induced an accelerated heart failure phenotype in the  
48  
49 young AnkBp.E1458G<sup>+/+</sup> mice (Figure 8). Overall, stress-inducing studies support our  
50  
51 hypothesis that the AnkBp.E1458G variant may be more likely to manifest with a  
52  
53  
54  
55  
56  
57  
58  
59  
60  
61  
62  
63  
64  
65

1  
2  
3  
4 cardiac phenotype in response to environmental stressors and aging. Similar results  
5  
6 were reported in a truncated Plakophilin-2 (PKP2) mouse model (p.R735X).  
7  
8 Plakophilin 2 variants are the most common ACM-causing genetic variants,  
9  
10 accounting for 23-58% of all ACM cases. However, the ACM phenotype did not  
11  
12 manifest in the PKP2p.R735X transgenic mice until exposure to eight weeks of  
13  
14 endurance exercise training (another environmental stressor) (27,28).  
15  
16  
17  
18

19  
20 Previous studies have shown NKA and AnkB dissociation as a prominent  
21  
22 mechanism for myocardial cell death after myocardial ischemia (29). Calpain-  
23  
24 mediated degradation of the NKA anchorage to the membrane cytoskeleton resulted  
25  
26 in  $\text{Na}^+$  overload, which had a secondary effect on NCX resulting in secondary  $\text{Ca}^{2+}$   
27  
28 overload within the cell following ischemia (29). Moreover, Skogestad et al. recently  
29  
30 demonstrated how disruption in the AnkB/NKA interaction resulted in increased  $\text{Ca}^{2+}$   
31  
32 sparks (30). Inhibition of NKA raises  $[\text{Na}^+]_i$ , and therefore influences the function of  
33  
34 NCX. In order to extrude excess  $\text{Na}^+$ ,  $[\text{Ca}^{2+}]_i$  becomes elevated, which can result in  
35  
36 altered  $\text{Ca}^{2+}$  cycling. Interestingly, Li et al. identified that inhibition of NKA during  
37  
38 stressed conditions can elicit pro-arrhythmic alternans in guinea pig cardiomyocytes  
39  
40 (31). Increased  $[\text{Ca}^{2+}]_i$  may result in calcium alternans that may translate into  
41  
42 conduction block and reentrant arrhythmia via non-uniform refractoriness throughout  
43  
44 the electrical signaling pathways (32).  
45  
46  
47  
48  
49  
50

51  
52 There are limitations to our work. Affected individuals in the setting of  
53  
54 AnkBp.E1458G have been in the heterozygous state. Notably, the phenotype of the  
55  
56 heterozygous mouse models (usually haploinsufficient) for desmosomal variants are  
57  
58 modest (often nothing is observed) and hence desmosomal genetic culprits are also  
59  
60  
61

1  
2  
3  
4 frequently studied in the homozygous state (33). Although gene dosage may be  
5  
6 higher, this mouse model still serves as an effective model for evaluating the potential  
7  
8 pathologies associated with this AnkB variant. A pressure overload model has not  
9  
10 previously been shown to predispose to ACM and to our knowledge, there is no  
11  
12 clinical data to suggest that pressure overload or hypertension exacerbates clinical  
13  
14 phenotype in the setting of an *ANK2* variant. Conclusions from this study should be  
15  
16 extrapolated with caution to other pathogenic human *ANK2* variants. Gene delivery  
17  
18 and pharmacological therapeutics can both be tested *in vivo* using this knock-in  
19  
20 model. While our studies were performed *in vivo*, it will be still crucial for expansion  
21  
22 of these studies into large animal models. Human induced pluripotent stem cells  
23  
24 (iPSCs) would best allow for specific excitation-contraction coupling and further Ca<sup>2+</sup>  
25  
26 regulation studies. In summary, while *ANK2* variants may be loss of function in vitro  
27  
28 or even in animal models, our findings support that secondary genetic or  
29  
30 environmental factors should be carefully assessed in the context of an ultimate  
31  
32 human clinical phenotype.  
33  
34  
35  
36  
37  
38  
39  
40

## 41 **Experimental Procedures**

### 42 **Mice**

43  
44  
45 A knock-in (KI) mouse to mimic the human variant at amino acid 1458 of human  
46  
47 *ANK2* was generated by The University of Michigan Transgenic Animal Model Core.  
48  
49 A single guide RNA (gRNA) was designed to create a CRISPR-induced indel in a  
50  
51 region close to codon 1371 in mouse (which corresponds to 1458 in human  
52  
53 sequence, ENSMUST00000182078.9). The gRNA along with Cas9 were  
54  
55 microinjected into C57BL/6J and SJL/J zygotes. Chimera mice were screened for the  
56  
57  
58  
59  
60  
61  
62  
63  
64  
65

1  
2  
3  
4 single amino acid substitution at the guide sequence. Germline mice were generated  
5  
6 by breeding chimeras to C57BL6/J mice. After germline transmission, mice were  
7  
8 genotyped and sequenced to confirm the substitution of the Glutamic acid amino acid  
9  
10 (E) for Glycine (G) (Forward: TGTAGACCAGTCCACCAGACACATT; Reverse:  
11  
12 CCCTGTCTAATTTCTCTAAAGTCAGAGGC). Mice were backcrossed on a  
13  
14 C57BL/6 background for five generations. The whole colony was produced from a  
15  
16 single founder. Age-matched male and female mice were used in experiments  
17  
18 throughout the manuscript. All animal experiments were conducted in accordance  
19  
20 with the Ohio State University Institutional Animal Care and Use Committee  
21  
22 guidelines (IACUC Protocol Number 2011A00000034).  
23  
24  
25  
26  
27  
28

### 29 **Echocardiography**

30  
31  
32 Transthoracic echocardiography using (GE Logiq e) with the L10-22 (mHz)  
33  
34 transducer was performed on mice anesthetized using 2% isoflurane in 95% O<sub>2</sub> and  
35  
36 5% CO<sub>2</sub>. Anesthesia was maintained by administration of oxygen and approximately  
37  
38 1.25% isoflurane during the whole imaging procedure. Heart rate (HR) was monitored  
39  
40 throughout imaging and recordings taken at a HR less than 400bpm were excluded  
41  
42 from the analysis. Mice were immobilized on a heated imaging stage during image  
43  
44 acquisition and a temperature probe was inserted into the rectum of the mouse to  
45  
46 monitor its core temperature of approximately 37°C. Electrode gel was placed on the  
47  
48 ECG sensors of the heated platform. Parasternal long-axis images inclusive of two-  
49  
50 dimensional loops and freeze-frame end-diastolic images were collected to measure  
51  
52 end-diastolic LV cavity dimension (LVID, d), and posterior wall thickness (LVPW, d).  
53  
54 Parasternal short axis images at the level of papillary muscles using M-mode were  
55  
56  
57  
58  
59  
60  
61  
62  
63  
64  
65

1  
2  
3  
4 also collected to determine LVPW and LVID, in both systole (s) and diastole (d), as  
5  
6 previously described (34). Parasternal long axis and M mode measurements were  
7  
8 used to calculate functional parameters including fractional shortening (FS%) and  
9  
10 ejection fraction (EF%).  
11  
12  
13

## 14 **Electrocardiogram**

15  
16  
17  
18 Surface electrocardiogram analysis was conducted on mice anesthetized with  
19  
20 isoflurane (2% in 1L/min oxygen). Anesthesia was maintained by administration of  
21  
22 oxygen and approximately 1% isoflurane during the whole recording procedure. Mice  
23  
24 were immobilized on a heated imaging stage during acquisition. Lead II ECGs were  
25  
26 collected using PowerLab equipment (AD Instruments). Subsurface ECG recordings  
27  
28 were collected from anesthetized mice around three months of age for a 5-min  
29  
30 interval of recording. Mice at ~three months of age were stimulated with epinephrine  
31  
32 (2mg/kg) under isoflurane sedation and ventricular arrhythmic events were calculated  
33  
34 over a 30-min period. Conscious ECGs were also collected using implanted radio-  
35  
36 telemetry devices using an ETA-F10 miniature telemeter (DSI) and Dataquest A.R.T  
37  
38 acquisition software around six months of age for baseline and post stimulation  
39  
40 measurements. All conscious ECGs were analyzed using LabChart software.  
41  
42 Researchers blinded to genotype performed data collection and analysis. Conscious  
43  
44 mice were stimulated with epinephrine (2mg/kg). After a week of rest, mice were  
45  
46 stimulated with epinephrine (2mg/kg) and caffeine (120mg/kg, Millipore Sigma  
47  
48 C1778) at the same time. ECG recordings were collected before stimulation to  
49  
50 measure baseline ECG features. Mice were then recorded for an hour post-  
51  
52 stimulation. The total number of ventricular arrhythmic events were calculated by  
53  
54  
55  
56  
57  
58  
59  
60  
61  
62  
63  
64  
65

1  
2  
3  
4 combining the number of arrhythmic events such as bigeminy (>10 consecutive  
5 abnormal ventricular beats alternating with normal ventricular beats), ventricular  
6  
7 tachycardia (>10 consecutive beats of tachycardia), non-sustained ventricular  
8  
9 tachycardia (three to ten consecutive beats), and isolated ventricular arrhythmic  
10  
11 events such as premature ventricular contractions (PVCs) and ventricular couplets.  
12  
13  
14

## 15 16 17 **Immunoblotting** 18 19

20 Heart tissue samples were isolated from seven-week and six-month old mice  
21  
22 after being euthanized using CO<sub>2</sub> and homogenized using a Cryolys-cooled Precellys  
23  
24 24 bead homogenizer (Bertin Corp.) using a combination of 1.4mm and 2.8mm  
25  
26 ceramic beads at 6000rpm for three bouts of 15 seconds in homogenization buffer  
27  
28 (0.025M Tris-HCl, 0.15M NaCl, 0.001M EDTA, 1% v/v NP-40, 5% v/v glycerol,  
29  
30 pH=7.4), as previously described (35). Homogenates were then centrifuged for 30  
31  
32 minutes at high speed at 4°C. Following quantification by BCA assay (Pierce), 30-  
33  
34 40ug of lysates were separated on 4-15% precast ProteanTGX gels (Bio-Rad) and  
35  
36 transferred to nitrocellulose membranes. Membranes were blocked at room  
37  
38 temperature for 1 hour and then incubated in primary antibody overnight at 4°C.  
39  
40 Primary antibodies targeted Ankyrin-B (1:1000, Covance antibody) (7), Na<sup>+</sup>/Ca<sup>2+</sup>  
41  
42 exchanger 1 (NCX1) (1:1000, Cell Signaling Technology CST 79350), NKA (1:1000,  
43  
44 Cell Signaling Technology CST 3010), and Ankyrin-G (1:1000, Covance, a gift from  
45  
46 Dr. Paul Jenkins) (36). Secondary antibodies used were donkey anti-rabbit or donkey  
47  
48 anti-mouse (Jackson ImmunoResearch Laboratories, Bio-Rad). Densitometry  
49  
50 analysis was performed using ImageJ software.  
51  
52  
53  
54  
55  
56  
57  
58  
59

## 60 **Histologic analysis** 61 62 63 64 65

1  
2  
3  
4 Hearts were excised and fixed in 10% neutral buffered formalin for 24 hours and  
5  
6 then stored in 100% ethanol at 4° C until sectioning. Masson's trichrome staining was  
7  
8 performed on 5µm sections at the histology core at the Wexner Medical Center at the  
9  
10 Ohio State University. Trichrome-stained cardiac sections were collected on an  
11  
12 EVOS microscope (Thermo Scientific). Researchers blinded to genotype performed  
13  
14 image collection and analysis. Whole-heart images were edited in Adobe Photoshop  
15  
16 to excise aortic tissue, as the focus of the study is intra-myocardial fibrosis. Fibrosis  
17  
18 was quantified using an add-on to MATLAB (Mathworks). The add-on converts  
19  
20 images from the RGB color space into CIELAB color space, then segments images  
21  
22 using the kmeans algorithm as previously described (35). Finally, the fibrosis (blue)  
23  
24 segment is filtered through a color mask to remove noise, and the ratio of fibrosis to  
25  
26 healthy red tissue is calculated.  
27  
28  
29  
30  
31  
32

### 33 **Isolation of cardiomyocytes**

34  
35  
36  
37 Adult mouse ventricular cardiomyocytes were prepared as previously described  
38  
39 (37). Murine hearts from male and female mice were obtained after animals were  
40  
41 euthanized by CO<sub>2</sub> asphyxiation followed by cervical dislocation in accordance with  
42  
43 the Guide for the Care and Use of Laboratory Animals published by the National  
44  
45 Institutes of Health and the Ohio State University Institutional Animal Care and Use  
46  
47 Committee-approved protocols. Following isolation, cells were fixed in ethanol and  
48  
49 stored at -20°C till staining experiments.  
50  
51  
52  
53

### 54 **Immunofluorescence**

1  
2  
3  
4 Adult ventricular myocytes were isolated, and processed for  
5  
6 immunofluorescence as previously described (38). For adult ventricular myocytes,  
7  
8 staining experiments were performed in solution. Briefly, cells were blocked for 1 hour  
9  
10 in blocking solution (3% fish gel, 0.75% triton-100(10%) and 1% DMSO). Cells were  
11  
12 incubated in primary antibodies at 4°C overnight while rotating. Primary antibodies  
13  
14 included NCX (Swant R3F1, 1:100), Ankyrin-B (1:100, Covance antibody) (7) and  
15  
16 NKA (Abcam ab7671, 1:100). Secondary antibodies, including anti-rabbit and anti-  
17  
18 mouse conjugated to Alexa-Fluor, were applied to the samples for 2 hours at room  
19  
20 temperature. For control experimental, parallel samples were incubated with  
21  
22 secondary antibodies and with primary antibody controls for 2 hours at room  
23  
24 temperature and processed to ensure lack of non-specific secondary antibody  
25  
26 staining. After secondary antibody incubation for 2 hours, cells were extensively  
27  
28 washed, applied to the slides in Vectashield imaging medium (Vector Laboratories,  
29  
30 Newark, CA, USA), and then coverslips (#1) were applied. Images were collected on  
31  
32 a confocal microscope (LSM 510 Meta, Zeiss, Oberkochen, Germany). Images were  
33  
34 collected using identical confocal protocol settings at room temperature, and the  
35  
36 observer was blinded to the genotype. Quantification of signal intensity was  
37  
38 performed using image J software. Area of overlap between two signals was  
39  
40 calculated using ROI (region of interest) manager under Image J software. All  
41  
42 calculations were normalized to control.  
43  
44  
45  
46  
47  
48  
49  
50  
51

### 52 53 **Detection of cytosolic Ca<sup>2+</sup> by confocal microscopy**

54  
55 Control or AnkBp.E1458G<sup>+/+</sup> myocytes were loaded with 10 μM Fluo-4-AM  
56  
57 (Thermo Fisher Scientific, MA, United States) for 20 minutes at RT. After 10-20  
58  
59  
60  
61

1  
2  
3  
4 minutes of de-esterification in free dye solution, the myocytes were mounted in an  
5  
6 imaging chamber (Warner Instruments, CT, United States) and continuously  
7  
8 superfused with an external solution containing (in mM): 137.0 NaCl, 5.4 KCl, 4.5  
9  
10 MgCl<sub>2</sub>, 0.16 NaH<sub>2</sub>PO<sub>4</sub>, 3 NaHCO<sub>3</sub>, 20.0 HEPES, 10.0 glucose, 10.4 taurine, 1.8  
11  
12 CaCl<sub>2</sub>. Intracellular Ca<sup>2+</sup> transients were induced by electrical field stimulation (SD9  
13  
14 stimulator, Grass Technologies/Astro-Med Inc., RI, United States). After stabilization  
15  
16 (usually 3–5 min) imaging was performed using Olympus FluoView FV 1000  
17  
18 (Olympus America Inc., PA, United States) confocal microscope system equipped  
19  
20 with x60 oil-immersion objective lens (NA 1.4). Fluo-4 was excited with a 488 nm line  
21  
22 of argon laser, and the signal was collected at 500–600 nm wavelengths. Line-  
23  
24 scanning (512 × 512 pixels, 2.0 μS/pixel and 2.1 msec per line) was performed along  
25  
26 the longitudinal axis of cells (avoiding nuclei). Fluorescence signals were normalized  
27  
28 to the baseline cellular fluorescence (F<sub>0</sub>). Ca<sup>2+</sup> transients were analyzed as the F/F<sub>0</sub>  
29  
30 mean value over 10-15 transients for each image. In the experiments with  
31  
32 Isoproterenol (ISO) treatment, the drug was administered to the perfusion buffer.  
33  
34 Spontaneous Ca<sup>2+</sup> waves were evaluated during 35 sec after stimulation at 2 Hz.  
35  
36 Ca<sup>2+</sup> alternans were induced incrementally by increasing the pacing frequency (1 to  
37  
38 5 Hz).  
39  
40  
41  
42  
43  
44  
45  
46  
47

### 48 **Transverse aortic constriction**

49

50  
51  
52 Mice were anesthetized with 2% isoflurane and intubated for artificial ventilation  
53  
54 at 120–160 breaths per minute, tidal volume of 0.2–0.35 ml. A Heating pad was used  
55  
56 to keep body temperatures at 37 °C throughout the procedure. The procedure was  
57  
58 performed on three-month-old mice as previously described (35). Briefly, the  
59  
60  
61  
62  
63  
64  
65

1  
2  
3  
4 transverse aorta was accessed via a left lateral thoracotomy and the aorta was ligated  
5  
6  
7 overlying a blunted 27-gauge needle. The needle was removed immediately following  
8  
9 ligation leaving a discrete region of stenosis at the aorta. Successful constriction was  
10  
11 confirmed by checking the aortic root and the constriction site using  
12  
13 echocardiography. The surgeon was blinded to genotype.  
14  
15

### 16 17 **Quantitative real-time PCR**

18  
19  
20 Real-time PCR was performed as previously described (34). Briefly, total RNA  
21  
22 from the mouse heart tissues was extracted with TRIzol Reagent (Invitrogen)  
23  
24 following manufacturer's instructions; 1 µg of total RNA, treated with ezDNase, was  
25  
26 used for the first-strand complementary DNA synthesis using SuperScript IV Vilo  
27  
28 Master Mix (Thermo Fisher Scientific). qRT-PCR reactions were performed in  
29  
30 triplicate in 96-well optical plates with PowerUp SYBR Green Master Mix (Thermo  
31  
32 Fisher Scientific). Primers for *Ank2*- F: TACAACCAACGTGTCTGCCA and R:  
33  
34 TGCAAAGGCAACAGACTCCT; *Nppa*- F: 5'-CTGGAAGTGGGAGGTCAAC-3', R: 5'-  
35  
36 AGGGCAGATCTATCGGAGGG-3'; *Nppb*- F: 5'-GCTCCCAATCCATCACAGA-3',  
37  
38 R: 5'-CTGCCTTGAGACCGAAGGAC-3'; *Myh7*- F: 5-  
39  
40 TGACAGAGGAGATGGCTGGT-3', R: 5'-CCTTGGCCTTGGTCAGAGTA-3';  
41  
42 *Col1a1*- F: 5'-TCCTTCCTCTACACAGGGTCC-3', R: 5'-  
43  
44 CGGCCACCATCTTGAGACTT-3'; *Timp1*- F: 5'-GGCATCTGGCATCCTCTTGT-3',  
45  
46 R: 5'-CAGGTCCGAGTTGCAGAAGG-3'. *Hprt* levels were used as a normalization  
47  
48 control.  
49  
50  
51  
52  
53  
54  
55

### 56 57 **Fast Fourier Transformation (FFT) Analysis**

1  
2  
3  
4 Heart rate variability was measured via fast Fourier transformation (FFT) based  
5  
6 time- and frequency-domain analysis. Custom MATLAB script (39) allowed FFT  
7  
8 analysis of text files with every raw RR interval within a period of time. To prepare  
9  
10 data for MATLAB analysis, ECG recordings were edited on Lab chart, and all noise  
11  
12 was removed. Each RR interval was then measured by Lab chart and exported into  
13  
14 a text file in 2-minute increments to screen for potential noise missed in the initial edit.  
15  
16 A total of 14 minutes was analyzed for RR and SDRR intervals and also FFT analyzed  
17  
18 to determine low-frequency (LF) and high-frequency (HF) spectra, LF/HF, etc. (LF  
19  
20 range 0.15-1.5 Hz, HF range 1.5-5 Hz).  
21  
22  
23  
24  
25

## 26 **Immunoprecipitation**

27  
28  
29 Control and AnkBp.E1458G<sup>+/+</sup> mouse heart samples were homogenized in  
30  
31 buffer (containing 0.025 m Tris-HCl, 0.15 m NaCl, 0.001 m EDTA, 1% (v/v) Nonidet  
32  
33 P-40, 5% (v/v) glycerol, pH 7.4) using the bead homogenizer. Lysates were  
34  
35 centrifuged for 30 min at 13,000 rpm at 4 °C. 400µg of supernatant was incubated  
36  
37 and rotated with AnkB-Ig (Covance, custom-made antibody) or control IgG at 4 °C  
38  
39 overnight. Following incubation, lysates with antibodies were rotated and incubated  
40  
41 with Protein A/G Magnetic Beads (Pierce, number 88802) for 4-5 h at 4 °C. The  
42  
43 supernatant was then removed from the beads using a magnetic stand, and the  
44  
45 beads were washed 3 times with PBS containing 500mM NaCl. Bound protein was  
46  
47 eluted with 2× Laemmli sample buffer and β-mercaptoethanol and heated to 95 °C  
48  
49 for 10 min before immunoblotting with NKA (1:750, Cell Signaling Technology CST  
50  
51 3010).  
52  
53  
54  
55  
56  
57  
58

## 59 **Statistics**

1  
2  
3  
4 Data are presented as mean  $\pm$  SEM. For the comparison of two groups, we  
5  
6 performed unpaired two-tailed student t-test when data passed normality test  
7  
8 (Shapiro-Wilk normality test). When data did not pass Shapiro-Wilk normality test, we  
9  
10 performed Mann-Whitney U test (non-parametric for unpaired comparison) to  
11  
12 compare two groups. For comparison of more than 2 groups, ANOVA test was  
13  
14 performed when data passed Shapiro-Wilk normality test followed by Tukey's  
15  
16 multiple comparisons test. When data did not pass Shapiro-Wilk normality test,  
17  
18 Kruskal-Wallis test (non-parametric) was performed followed by Dunn's multiple  
19  
20 comparisons test. For cardiac function parameters (EF, FS, LVIDd, LVIDs) measured  
21  
22 over time in response to TAC, data was screened graphically with model residuals,  
23  
24 homoskedasticity, and QQ plots to ensure the applicability of a two-way ANOVA. A  
25  
26 two-way ANOVA mixed effects model for repeated measures was then used with  
27  
28 post-hoc Holm-Šídák multiple comparisons test. Sphericity was not assumed, and  
29  
30 the Geisser-Greenhouse correction was deployed. For our study, a value of  $p < 0.05$   
31  
32 was considered statistically significant.  
33  
34  
35  
36  
37  
38  
39  
40

#### 41 **Data availability**

42 All data are available within the manuscript or supporting information.  
43  
44

#### 45 **Supporting information**

46 This article contains supporting information.  
47  
48

#### 49 **Acknowledgements**

50  
51  
52  
53  
54  
55  
56  
57  
58  
59  
60  
61  
62  
63  
64  
65

1  
2  
3  
4 The authors would like to acknowledge the University of Michigan Transgenic Animal  
5  
6 Model Core for their help in the generation of the AnkBp.E1458G murine model. The  
7  
8 authors would also like to acknowledge the Ohio State University College of  
9  
10 Veterinary Medicine Comparative Pathology & Digital Imaging Shared Resource for  
11  
12 their assistance with histology services.  
13  
14

### 15 16 17 **Funding**

18  
19  
20 The authors are supported by NIH grants, HL146969 to M.E.R., HL135754 to P.J.M.,  
21  
22 HL156652 to T.J.H., HL063043, HL074045 to S.G., a grant from the Ohio State Frick  
23  
24 Center for Heart Failure and Arrhythmia and the Leducq Foundation (TNE FANTASY  
25  
26 19CV03) to P.J.M. and M.E.M. The content is solely the responsibility of the authors  
27  
28 and does not necessarily represent the official views of the National Institutes of  
29  
30 Health.  
31  
32  
33

### 34 35 36 **Conflict of Interest**

37  
38  
39 The authors declare that they have no conflicts of interest with the contents of this  
40  
41 article.  
42  
43

### 44 45 46 **Author contributions**

47  
48 M.E.R. and P.J.M. conceived and designed the project; M.E.R., M.J.W., J.I.M. , M.H.,  
49  
50 L.J.Y., T.L.S., S.A-B., N.M., D.A., O.C., S.S.T., N.P.M. and X.X. performed  
51  
52 experiments; M.E.R., M.J.W., J.I.M., O.C., S.S.T., L.J.Y., S.A.-B. analyzed data;  
53  
54 M.E.R, M.J.W., J.I.M., T.L.S., J.D.R, T.J.H., M.E.M., S.G. and P.J.M. interpreted the  
55  
56 results of experiments; M.E.R., J.I.M. and M.J.W. prepared figures; M.E.R., M.J.W.,  
57  
58  
59  
60  
61  
62  
63  
64  
65

1  
2  
3  
4 J.I.M., J.D.R., S.G. and P.J.M. drafted the manuscript. All authors have contributed  
5  
6 and agreed to the final version of the manuscript.  
7  
8  
9

## 10 **References**

- 11  
12  
13 1. Scotland, P., Zhou, D., Benveniste, H., and Bennett, V. (1998) Nervous  
14 system defects of AnkyrinB (-/-) mice suggest functional overlap between the  
15 cell adhesion molecule L1 and 440-kD AnkyrinB in premyelinated axons. *J*  
16 *Cell Biol* **143**, 1305-1315  
17  
18
- 19 2. Cunha, S. R., Bhasin, N., and Mohler, P. J. (2007) Targeting and stability of  
20 Na/Ca exchanger 1 in cardiomyocytes requires direct interaction with the  
21 membrane adaptor ankyrin-B. *J Biol Chem* **282**, 4875-4883  
22  
23
- 24 3. Koenig, S. N., and Mohler, P. J. (2017) The evolving role of ankyrin-B in  
25 cardiovascular disease. *Heart Rhythm* **14**, 1884-1889  
26  
27
- 28 4. Cunha, S. R., Le Scouarnec, S., Schott, J. J., and Mohler, P. J. (2008) Exon  
29 organization and novel alternative splicing of the human ANK2 gene:  
30 implications for cardiac function and human cardiac disease. *J Mol Cell Cardiol*  
31 **45**, 724-734  
32  
33
- 34 5. Lopes, L. R., Syrris, P., Guttman, O. P., O'Mahony, C., Tang, H. C.,  
35 Dalageorgou, C., Jenkins, S., Hubank, M., Monserrat, L., McKenna, W. J.,  
36 Plagnol, V., and Elliott, P. M. (2015) Novel genotype-phenotype associations  
37 demonstrated by high-throughput sequencing in patients with hypertrophic  
38 cardiomyopathy. *Heart* **101**, 294-301  
39  
40  
41  
42  
43  
44  
45  
46  
47  
48  
49  
50  
51  
52  
53  
54  
55  
56  
57  
58  
59  
60  
61  
62  
63  
64  
65

- 1  
2  
3  
4  
5  
6  
7  
8  
9  
10  
11  
12  
13  
14  
15  
16  
17  
18  
19  
20  
21  
22  
23  
24  
25  
26  
27  
28  
29  
30  
31  
32  
33  
34  
35  
36  
37  
38  
39  
40  
41  
42  
43  
44  
45  
46  
47  
48  
49  
50  
51  
52  
53  
54  
55  
56  
57  
58  
59  
60  
61  
62  
63  
64  
65
6. Curran, J., and Mohler, P. J. (2011) Coordinating electrical activity of the heart: ankyrin polypeptides in human cardiac disease. *Expert Opin Ther Targets* **15**, 789-801
  7. Roberts, J. D., Murphy, N. P., Hamilton, R. M., Lubbers, E. R., James, C. A., Kline, C. F., Gollob, M. H., Krahn, A. D., Sturm, A. C., Musa, H., El-Refaey, M., Koenig, S., Aneq, M. A., Hoorntje, E. T., Graw, S. L., Davies, R. W., Rafiq, M. A., Koopmann, T. T., Aafaqi, S., Fatah, M., Chiasson, D. A., Taylor, M. R., Simmons, S. L., Han, M., van Opbergen, C. J., Wold, L. E., Sinagra, G., Mittal, K., Tichnell, C., Murray, B., Codima, A., Nazer, B., Nguyen, D. T., Marcus, F. I., Sobriera, N., Lodder, E. M., van den Berg, M. P., Spears, D. A., Robinson, J. F., Ursell, P. C., Green, A. K., Skanes, A. C., Tang, A. S., Gardner, M. J., Hegele, R. A., van Veen, T. A., Wilde, A. A., Healey, J. S., Janssen, P. M., Mestroni, L., van Tintelen, J. P., Calkins, H., Judge, D. P., Hund, T. J., Scheinman, M. M., and Mohler, P. J. (2019) Ankyrin-B dysfunction predisposes to arrhythmogenic cardiomyopathy and is amenable to therapy. *J Clin Invest* **129**, 3171-3184
  8. Choi, C. S. W., Souza, I. A., Sanchez-Arias, J. C., Zamponi, G. W., Arbour, L. T., and Swayne, L. A. (2019) Ankyrin B and Ankyrin B variants differentially modulate intracellular and surface Cav2.1 levels. *Mol Brain* **12**, 75
  9. Lin, Y., Williams, N., Wang, D., Coetzee, W., Zhou, B., Eng, L. S., Um, S. Y., Bao, R., Devinsky, O., McDonald, T. V., Sampson, B. A., and Tang, Y. (2017) Applying High-Resolution Variant Classification to Cardiac Arrhythmogenic

1  
2  
3  
4 Gene Testing in a Demographically Diverse Cohort of Sudden Unexplained  
5 Deaths. *Circ Cardiovasc Genet* **10**  
6  
7

- 8  
9  
10 10. Hedley, P. L., Jorgensen, P., Schlamowitz, S., Wangari, R., Moolman-Smook,  
11 J., Brink, P. A., Kanters, J. K., Corfield, V. A., and Christiansen, M. (2009) The  
12 genetic basis of long QT and short QT syndromes: a mutation update. *Hum*  
13 *Mutat* **30**, 1486-1511  
14  
15  
16  
17  
18 11. Mitchell, G. F., Jeron, A., and Koren, G. (1998) Measurement of heart rate and  
19 Q-T interval in the conscious mouse. *Am J Physiol* **274**, H747-751  
20  
21  
22  
23 12. Mulla, W., Murninkas, M., Levi, O., and Etzion, Y. (2022) Incorrectly corrected?  
24 QT interval analysis in rats and mice. *Front Physiol* **13**, 1002203  
25  
26  
27  
28 13. Roussel, J., Champeroux, P., Roy, J., Richard, S., Fauconnier, J., Le  
29 Guennec, J. Y., and Thireau, J. (2016) The Complex QT/RR Relationship in  
30 Mice. *Sci Rep* **6**, 25388  
31  
32  
33  
34  
35 14. Kmecova, J., and Klimas, J. (2010) Heart rate correction of the QT duration in  
36 rats. *Eur J Pharmacol* **641**, 187-192  
37  
38  
39  
40 15. Billman, G. E. (2013) The LF/HF ratio does not accurately measure cardiac  
41 sympatho-vagal balance. *Front Physiol* **4**, 26  
42  
43  
44  
45 16. Laurita, K. R., and Rosenbaum, D. S. (2008) Cellular mechanisms of  
46 arrhythmogenic cardiac alternans. *Prog Biophys Mol Biol* **97**, 332-347  
47  
48  
49  
50 17. Florea, S. M., and Blatter, L. A. (2012) Regulation of cardiac alternans by beta-  
51 adrenergic signaling pathways. *Am J Physiol Heart Circ Physiol* **303**, H1047-  
52 1056  
53  
54  
55  
56  
57  
58  
59  
60  
61  
62  
63  
64  
65

- 1  
2  
3  
4 18. Hammer, K. P., Ljubojevic, S., Ripplinger, C. M., Pieske, B. M., and Bers, D.  
5  
6 M. (2015) Cardiac myocyte alternans in intact heart: Influence of cell-cell  
7  
8 coupling and beta-adrenergic stimulation. *J Mol Cell Cardiol* **84**, 1-9  
9  
10  
11 19. Le Scouarnec, S., Bhasin, N., Vieyres, C., Hund, T. J., Cunha, S. R., Koval,  
12  
13 O., Marionneau, C., Chen, B., Wu, Y., Demolombe, S., Song, L. S., Le Marec,  
14  
15 H., Probst, V., Schott, J. J., Anderson, M. E., and Mohler, P. J. (2008)  
16  
17 Dysfunction in ankyrin-B-dependent ion channel and transporter targeting  
18  
19 causes human sinus node disease. *Proc Natl Acad Sci U S A* **105**, 15617-  
20  
21 15622  
22  
23  
24  
25 20. Hertz, C. L., Christiansen, S. L., Larsen, M. K., Dahl, M., Ferrero-Miliani, L.,  
26  
27 Weeke, P. E., Pedersen, O., Hansen, T., Grarup, N., Ottesen, G. L., Frank-  
28  
29 Hansen, R., Banner, J., and Morling, N. (2016) Genetic investigations of  
30  
31 sudden unexpected deaths in infancy using next-generation sequencing of  
32  
33 100 genes associated with cardiac diseases. *Eur J Hum Genet* **24**, 817-822  
34  
35  
36  
37 21. Neubauer, J., Lecca, M. R., Russo, G., Bartsch, C., Medeiros-Domingo, A.,  
38  
39 Berger, W., and Haas, C. (2017) Post-mortem whole-exome analysis in a large  
40  
41 sudden infant death syndrome cohort with a focus on cardiovascular and  
42  
43 metabolic genetic diseases. *Eur J Hum Genet* **25**, 404-409  
44  
45  
46  
47 22. Reuter, M. S., Walker, S., Thiruvahindrapuram, B., Whitney, J., Cohn, I.,  
48  
49 Sondheimer, N., Yuen, R. K. C., Trost, B., Paton, T. A., Pereira, S. L., Herbrick,  
50  
51 J. A., Wintle, R. F., Merico, D., Howe, J., MacDonald, J. R., Lu, C.,  
52  
53 Nalpathamkalam, T., Sung, W. W. L., Wang, Z., Patel, R. V., Pellicchia, G.,  
54  
55 Wei, J., Strug, L. J., Bell, S., Kellam, B., Mahtani, M. M., Bassett, A. S.,  
56  
57  
58  
59  
60  
61  
62  
63  
64  
65

1  
2  
3  
4 Bombard, Y., Weksberg, R., Shuman, C., Cohn, R. D., Stavropoulos, D. J.,  
5  
6 Bowdin, S., Hildebrandt, M. R., Wei, W., Romm, A., Pasceri, P., Ellis, J., Ray,  
7  
8 P., Meyn, M. S., Monfared, N., Hosseini, S. M., Joseph-George, A. M., Keeley,  
9  
10 F. W., Cook, R. A., Fiume, M., Lee, H. C., Marshall, C. R., Davies, J., Hazell,  
11  
12 A., Buchanan, J. A., Szego, M. J., and Scherer, S. W. (2018) The Personal  
13  
14 Genome Project Canada: findings from whole genome sequences of the  
15  
16 inaugural 56 participants. *CMAJ* **190**, E126-E136  
17  
18  
19  
20

21 23. Ware, J. S., Walsh, R., Cunningham, F., Birney, E., and Cook, S. A. (2012)  
22  
23 Paralogous annotation of disease-causing variants in long QT syndrome  
24  
25 genes. *Hum Mutat* **33**, 1188-1191  
26  
27

28 24. Adler, A., Novelli, V., Amin, A. S., Abiusi, E., Care, M., Nannenber, E. A.,  
29  
30 Feilotter, H., Amenta, S., Mazza, D., Bikker, H., Sturm, A. C., Garcia, J.,  
31  
32 Ackerman, M. J., Hershberger, R. E., Perez, M. V., Zareba, W., Ware, J. S.,  
33  
34 Wilde, A. A. M., and Gollob, M. H. (2020) An International, Multicentered,  
35  
36 Evidence-Based Reappraisal of Genes Reported to Cause Congenital Long  
37  
38 QT Syndrome. *Circulation* **141**, 418-428  
39  
40  
41  
42

43 25. Giudicessi, J. R., and Ackerman, M. J. (2020) Established Loss-of-Function  
44  
45 Variants in ANK2-Encoded Ankyrin-B Rarely Cause a Concerning Cardiac  
46  
47 Phenotype in Humans. *Circ Genom Precis Med* **13**, e002851  
48  
49

50 26. Sosnowski, M., and Petelenz, T. (1995) Heart rate variability. Is it influenced  
51  
52 by disturbed sinoatrial node function? *J Electrocardiol* **28**, 245-251  
53  
54

55 27. Cruz, F. M., Sanz-Rosa, D., Roche-Molina, M., Garcia-Prieto, J., Garcia-Ruiz,  
56  
57 J. M., Pizarro, G., Jimenez-Borreguero, L. J., Torres, M., Bernad, A., Ruiz-  
58  
59  
60  
61

1  
2  
3  
4 Cabello, J., Fuster, V., Ibanez, B., and Bernal, J. A. (2015) Exercise triggers  
5 ARVC phenotype in mice expressing a disease-causing mutated version of  
6 human plakophilin-2. *J Am Coll Cardiol* **65**, 1438-1450  
7  
8

9  
10  
11 28. Stevens, T. L., Wallace, M. J., Refaey, M. E., Roberts, J. D., Koenig, S. N.,  
12 and Mohler, P. J. (2020) Arrhythmogenic Cardiomyopathy: Molecular Insights  
13 for Improved Therapeutic Design. *J Cardiovasc Dev Dis* **7**  
14  
15

16  
17  
18 29. Inserte, J., Garcia-Dorado, D., Hernando, V., and Soler-Soler, J. (2005)  
19 Calpain-mediated impairment of Na<sup>+</sup>/K<sup>+</sup>-ATPase activity during early  
20 reperfusion contributes to cell death after myocardial ischemia. *Circ Res* **97**,  
21 465-473  
22  
23

24  
25  
26 30. Skogestad, J., Aronsen, J. M., Tovsrud, N., Wanichawan, P., Hougen, K.,  
27 Stokke, M. K., Carlson, C. R., Sjaastad, I., Sejersted, O. M., and Swift, F.  
28 (2020) Coupling of the Na<sup>+</sup>/K<sup>+</sup>-ATPase to Ankyrin B controls Na<sup>+</sup>/Ca<sup>2+</sup>  
29 exchanger activity in cardiomyocytes. *Cardiovasc Res* **116**, 78-90  
30  
31

32  
33  
34 31. Li, Q., Pogwizd, S. M., Prabhu, S. D., and Zhou, L. (2014) Inhibiting Na<sup>+</sup>/K<sup>+</sup>  
35 ATPase can impair mitochondrial energetics and induce abnormal Ca<sup>2+</sup>  
36 cycling and automaticity in guinea pig cardiomyocytes. *PLoS One* **9**, e93928  
37  
38

39  
40  
41 32. Landstrom, A. P., Dobrev, D., and Wehrens, X. H. T. (2017) Calcium Signaling  
42 and Cardiac Arrhythmias. *Circ Res* **120**, 1969-1993  
43  
44

45  
46  
47 33. Cerrone, M., Montnach, J., Lin, X., Zhao, Y. T., Zhang, M., Agullo-Pascual, E.,  
48 Leo-Macias, A., Alvarado, F. J., Dolgalev, I., Karathanos, T. V., Malkani, K.,  
49 Van Opbergen, C. J. M., van Bavel, J. J. A., Yang, H. Q., Vasquez, C., Tester,  
50 D., Fowler, S., Liang, F., Rothenberg, E., Heguy, A., Morley, G. E., Coetzee,  
51  
52  
53  
54  
55  
56  
57  
58  
59  
60  
61

1  
2  
3  
4 W. A., Trayanova, N. A., Ackerman, M. J., van Veen, T. A. B., Valdivia, H. H.,  
5  
6 and Delmar, M. (2017) Plakophilin-2 is required for transcription of genes that  
7  
8 control calcium cycling and cardiac rhythm. *Nat Commun* **8**, 106  
9

10  
11 34. Cavus, O., Williams, J., Musa, H., El Refaey, M., Gratz, D., Shaheen, R.,  
12  
13 Schwieterman, N. A., Koenig, S., Antwi-Boasiako, S., Young, L. J., Xu, X.,  
14  
15 Han, M., Wold, L. E., Hund, T. J., Mohler, P. J., and Bradley, E. A. (2021) Giant  
16  
17 ankyrin-G regulates cardiac function. *J Biol Chem* **296**, 100507  
18  
19

20  
21 35. Lubbers, E. R., Murphy, N. P., Musa, H., Huang, C. Y., Gupta, R., Price, M.  
22  
23 V., Han, M., Daoud, E., Gratz, D., El Refaey, M., Xu, X., Hoeflinger, N. K.,  
24  
25 Friel, E. L., Lancione, P., Wallace, M. J., Cavus, O., Simmons, S. L., Williams,  
26  
27 J. L., Skaf, M., Koenig, S. N., Janssen, P. M. L., Rasband, M. N., Hund, T. J.,  
28  
29 and Mohler, P. J. (2019) Defining new mechanistic roles for alphaII spectrin in  
30  
31 cardiac function. *J Biol Chem* **294**, 9576-9591  
32  
33

34  
35 36. Jenkins, P. M., Kim, N., Jones, S. L., Tseng, W. C., Svitkina, T. M., Yin, H. H.,  
36  
37 and Bennett, V. (2015) Giant ankyrin-G: a critical innovation in vertebrate  
38  
39 evolution of fast and integrated neuronal signaling. *Proc Natl Acad Sci U S A*  
40  
41 **112**, 957-964  
42  
43

44  
45 37. Koval, O. M., Snyder, J. S., Wolf, R. M., Pavlovicz, R. E., Glynn, P., Curran,  
46  
47 J., Leymaster, N. D., Dun, W., Wright, P. J., Cardona, N., Qian, L., Mitchell, C.  
48  
49 C., Boyden, P. A., Binkley, P. F., Li, C., Anderson, M. E., Mohler, P. J., and  
50  
51 Hund, T. J. (2012) Ca<sup>2+</sup>/calmodulin-dependent protein kinase II-based  
52  
53 regulation of voltage-gated Na<sup>+</sup> channel in cardiac disease. *Circulation* **126**,  
54  
55 2084-2094  
56  
57  
58  
59  
60  
61

- 1  
2  
3  
4 38. El Refaey, M., Coles, S., Musa, H., Stevens, T. L., Wallace, M. J., Murphy, N.  
5  
6 P., Antwi-Boasiako, S., Young, L. J., Manning, H. R., Curran, J., Makara, M.  
7  
8 A., Sas, K., Han, M., Koenig, S. N., Skaf, M., Kline, C. F., Janssen, P. M. L.,  
9  
10 Accornero, F., Borzok, M. A., and Mohler, P. J. (2022) Altered Expression of  
11  
12 Zonula occludens-1 Affects Cardiac Na(+) Channels and Increases  
13  
14 Susceptibility to Ventricular Arrhythmias. *Cells* **11**  
15  
16  
17  
18  
19 39. Bidaud, I., D'Souza, A., Forte, G., Torre, E., Greuet, D., Thirard, S., Anderson,  
20  
21 C., Chung You Chong, A., Torrente, A. G., Roussel, J., Wickman, K., Boyett,  
22  
23 M. R., Mangoni, M. E., and Mesirca, P. (2020) Genetic Ablation of G Protein-  
24  
25 Gated Inwardly Rectifying K(+) Channels Prevents Training-Induced Sinus  
26  
27 Bradycardia. *Front Physiol* **11**, 519382  
28  
29  
30

### 31 **Figure legends**

32  
33  
34  
35 **Figure 1. Creation of a novel AnkBp.E1458G knock-in mouse model. A.**  
36  
37 Diagrammatic illustration denoting the location of the variant in the spectrin-binding  
38  
39 domain of canonical ankyrin-B. **B-C** Representative Sanger sequencing  
40  
41 chromatogram denoting the amino acid sequence in the control and the  
42  
43 AnkBp.E1458G<sup>+/+</sup> mice and confirming the substitution of the Glutamic acid (E) by  
44  
45 Glycine (G) **D.** *Ank2* relative expression in control and AnkBp.E1458G<sup>+/+</sup> mice at  
46  
47 seven weeks of age (N=4 mice/genotype), data passed Shapiro-Wilk normality test  
48  
49 and unpaired t-test was performed. **E-F.** Immunoblotting and quantitative analysis of  
50  
51 normalized AnkB expression in the control and the AnkBp.E1458G<sup>+/+</sup> mice (N=4  
52  
53 mice/genotype), data passed Shapiro-Wilk normality test and unpaired t-test was  
54  
55  
56  
57  
58  
59  
60  
61  
62  
63  
64  
65

1  
2  
3  
4 performed. Red arrow denotes the change in the amino acid. Yellow arrows denote  
5  
6 the multiple silent coding changes to block the Cas9 targets.  
7  
8

9  
10 **Figure 2. AnkBp.E1458G<sup>+/+</sup> mice display a cardiac phenotype at ~six months of**

11 **age. A.** Control and AnkBp.E1458G<sup>+/+</sup> mice do not display changes in the ejection  
12 fraction around three months of age (young mice), data passed Shapiro-Wilk  
13 normality test and unpaired t-test was performed. **B-D.** Quantitative analysis and  
14 representative echocardiographs denoting a reduction in ejection fraction in the  
15 AnkBp.E1458G<sup>+/+</sup> vs. the control littermates at ~six months of age (Con, N=7 and  
16 AnkBp.E1458G<sup>+/+</sup>, N=11) Scale bars equal 2mm. Data passed Shapiro-Wilk  
17 normality test and unpaired t-test was performed. **E.** H&E staining and **F.** Masson  
18 Trichrome staining using control and AnkBp.E1458G<sup>+/+</sup> heart sections in aged mice  
19 (Con, N=4 and AnkBp.E1458G<sup>+/+</sup>, N=5). **G.** Heart weight relative to tibial length in the  
20 two groups of mice (Con, N=6 and AnkBp.E1458G<sup>+/+</sup>, N=7, around five months of  
21 age). Data passed Shapiro-Wilk normality test and unpaired t-test was performed. **H.**  
22 Quantitative analysis of fibrosis (Con, N=4 and AnkBp.E1458G<sup>+/+</sup>, N=5, around five  
23 months of age). Scale bars equal 1mm. Data passed Shapiro-Wilk normality test and  
24 unpaired t-test was performed.  
25  
26  
27  
28  
29  
30  
31  
32  
33  
34  
35  
36  
37  
38  
39  
40  
41  
42  
43  
44  
45

46  
47 **Figure 3. Aged AnkBp.E1458G<sup>+/+</sup> mice display electrical dysfunction at rest. A.**

48 Average heart rate, **B.** Maximal heart rate, **C.** P wave duration, **D.** PR interval, **E.**  
49 QRS interval, **F.** RR interval, **G.** QT interval and **H.** QTc (Mitchell) using radio-  
50 implanted telemeters in control and AnkBp.E1458G<sup>+/+</sup> mice around six months of age  
51 (Con, N=7 and AnkBp.E1458G, N=10). Data passed Shapiro-Wilk normality tests and  
52  
53  
54  
55  
56  
57  
58  
59  
60  
61  
62  
63  
64  
65

1  
2  
3  
4 unpaired t-tests were performed (A-G). Data did not pass Shapiro-Wilk normality test  
5  
6 and non-parametric (Mann-Whitney test) was performed.  
7  
8

9  
10 **Figure 4. Aged AnkBp.E1458G<sup>+/+</sup> mice display heart rate variability at rest. A.**

11 High frequency (HF) and **B.** Low frequency (LF) spectral components of heart rate  
12 variability HRV. Data did not pass Shapiro-Wilk normality tests and non-parametric  
13 (Mann-Whitney tests) were performed. **C.** LF/HF using Fast Fourier transform (FFT)  
14 analysis and radio-implanted telemeters in control and AnkBp.E1458G<sup>+/+</sup> mice  
15 around six months of age (Con, N=13 and AnkBp.E1458G<sup>+/+</sup>, N=16). Data passed  
16 Shapiro-Wilk normality test and unpaired t-test was performed. **D.** RR-Interval, data  
17 passed Shapiro-Wilk normality test and unpaired t-test was performed. **E.** SDRR-  
18 Interval, data did not pass Shapiro-Wilk normality test and non-parametric (Mann-  
19 Whitney test) was performed. **F.** representative traced from control and  
20 AnkBp.E1458G<sup>+/+</sup> mice over 1 min interval.  
21  
22  
23  
24  
25  
26  
27  
28  
29  
30  
31  
32  
33  
34  
35  
36

37 **Figure 5. AnkBp.E1458G<sup>+/+</sup> mice display arrhythmias following adrenergic**

38 **stimulation/stress. A.** AnkBp.E1458G<sup>+/+</sup> mice display ventricular arrhythmic events  
39 after epinephrine stimulation at an early age (~three months of age) under isoflurane  
40 sedation (Con, N=6 and AnkBp.E1458G<sup>+/+</sup>, N=6). Data did not pass Shapiro-Wilk  
41 normality test and non-parametric (Mann-Whitney test) was performed. **B-D.**  
42 Representative ECG traces denoting PVCs and chain of couplets in the  
43 AnkBp.E1458G<sup>+/+</sup> mice at early age after epinephrine stimulation and under  
44 isoflurane sedation.  
45  
46  
47  
48  
49  
50  
51  
52  
53  
54  
55  
56

57 **Figure 6. AnkBp.E1458G<sup>+/+</sup> mice display a significant pattern of arrhythmia after**

58 **epinephrine and caffeine stimulation. A.** AnkBp.E1458G<sup>+/+</sup> mice show more  
59  
60  
61  
62  
63  
64  
65

1  
2  
3  
4 ventricular arrhythmic events after epinephrine stimulation using implanted  
5  
6 telemeters around six months of age (Con, N=15 and AnkBp.E1458G<sup>+/+</sup>, N=22). Data  
7  
8 did not pass Shapiro-Wilk normality test and non-parametric (Mann-Whitney test)  
9  
10 was performed. **B.** AnkBp.E1458G<sup>+/+</sup> mice display significant increase in the number  
11  
12 of ventricular arrhythmic events after epinephrine and caffeine stimulation using  
13  
14 telemeters around six months of age (Con, N=6 and AnkBp.E1458G<sup>+/+</sup>, N=6). **C.**  
15  
16 AnkBp.E1458G<sup>+/+</sup> mice exhibit an increase in the number of sustained arrhythmic  
17  
18 events after epinephrine and caffeine stimulation (Con, N=6 and AnkBp.E1458G<sup>+/+</sup>,  
19  
20 N=6). Data passed Shapiro-Wilk normality tests and unpaired t-tests were performed  
21  
22 (B-C). **D.** AnkBp.E1458G<sup>+/+</sup> mice display longer episodes of the sustained events  
23  
24 after epinephrine and caffeine stimulation (Con, N=6 and AnkBp.E1458G<sup>+/+</sup>, N=6).  
25  
26 Data did not pass Shapiro-Wilk normality test and non-parametric (Mann-Whitney  
27  
28 test) was performed. **E.** AnkBp.E1458G<sup>+/+</sup> mice demonstrate a higher number of non-  
29  
30 sustained ventricular events (NSVT) after epinephrine and caffeine stimulation (Con,  
31  
32 N=6 and AnkBp.E1458G<sup>+/+</sup>, N=6). Data did not pass Shapiro-Wilk normality test and  
33  
34 non-parametric (Mann-Whitney test) was performed. **F-H.** Representative ECG  
35  
36 traces denoting non-sustained and sustained arrhythmic events in the  
37  
38 AnkBp.E1458G<sup>+/+</sup> mice after epinephrine and caffeine stimulation.  
39  
40  
41  
42  
43  
44  
45  
46  
47

48  
49 **Figure 7. Calcium handling in AnkBp.E1458G<sup>+/+</sup> myocytes. A.** Representative  
50  
51 confocal line-scan images and Ca<sup>2+</sup> transient profiles recorded in mouse ventricular  
52  
53 myocytes loaded with Fluo-4-AM and stimulated at 1 Hz, with or without 500 nM ISO  
54  
55 treatment in control (upper panel) and AnkBp.E1458G<sup>+/+</sup> (lower panel) myocytes. **B.**  
56  
57 Summary data on Ca<sup>2+</sup> transient amplitude and **C.** time constant of single exponential  
58  
59  
60  
61  
62  
63  
64  
65

1  
2  
3  
4 decay (Tau) in control and AnkBp.E1458G<sup>+/+</sup> myocytes with or without ISO treatment  
5  
6 at indicated doses. All groups were compared using paired mixed-effects ANOVA  
7  
8 followed by Tukey correction. P<0.05 vs control or AnkBp.E1458G<sup>+/+</sup> without  
9  
10 treatment was considered significant. N=5-7 animals per group (n=15-34 myocytes).  
11  
12 Shapiro-Wilk test was used to evaluate normal distribution. **D.** Representative  
13  
14 confocal line-scan images of control (upper panel) and AnkBp.E1458G<sup>+/+</sup> myocytes  
15  
16 (lower panel) showing spontaneous Ca<sup>2+</sup> waves in 35 seconds post-stimulation at 2  
17  
18 Hz. **E.** Comparison of the fraction of myocytes with spontaneous Ca<sup>2+</sup> waves in 35  
19  
20 seconds post-stimulation at 2 Hz in control and AnkBp.E1458G<sup>+/+</sup> mice with and  
21  
22 without ISO treatment. The presence or absence of spontaneous Ca<sup>2+</sup> waves was  
23  
24 analyzed using a two-tailed Chi-squared test. N=5-7 animals per group (n=12-36  
25  
26 myocytes). **F.** Representative confocal line-scan images of control (upper panel) and  
27  
28 AnkBp.E1458G<sup>+/+</sup> myocytes stimulated at 3 Hz, showing the presence of alternans  
29  
30 (lower panel). **G.** Summary data on the fraction of myocytes presenting alternans at  
31  
32 3 Hz or 4 Hz pacing frequency in control and AnkBp.E1458G<sup>+/+</sup> myocytes with or  
33  
34 without ISO treatment. The presence or absence of alternans was analyzed using a  
35  
36 two-tailed Chi-squared test. P<0.05 vs control in the same condition was considered  
37  
38 significant. N=4-5 animals per group (n=10-28 myocytes). **H.** Threshold frequency for  
39  
40 the development of alternans. Only myocytes that manifested alternans between 1-5  
41  
42 Hz were considered for this analysis. Control and AnkBp.E1458G<sup>+/+</sup> in each condition  
43  
44 were compared by student's t-test. P<0.05 vs control in the same condition was  
45  
46 considered significant. N=4-5 animals per group (n=7-14 myocytes).  
47  
48  
49  
50  
51  
52  
53  
54  
55  
56  
57  
58  
59  
60  
61  
62  
63  
64  
65

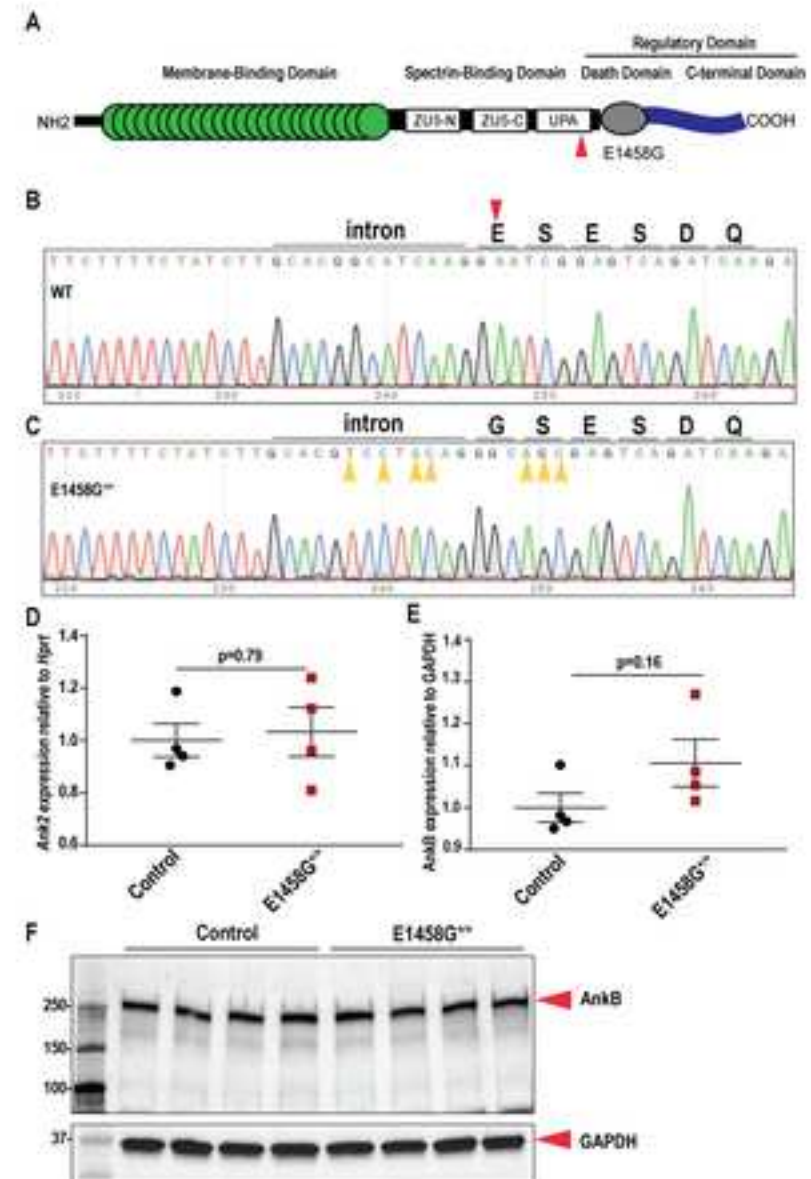
1  
2  
3  
4 **Figure 8. AnkBp.E1458G<sup>+/+</sup> mice display severe structural phenotype following**  
5 **pressure overload. A.** AnkBp.E1458G<sup>+/+</sup> mice display a reduction in the ejection  
6 fraction at eight and twelve weeks compared to control littermates post TAC surgery  
7 (Con and AnkBp.E1458G<sup>+/+</sup>, N=5-6). Repeated measures two-way ANOVA mixed  
8 effects model was performed (time effect: p<0.0001, F=69.98, genotype effect:  
9 p<0.05, F=6.52, time-genotype interaction effect: p<0.01, F=3.45) with Holm-Šídák  
10 multiple comparisons test represented in figure. **B.** AnkBp.E1458G<sup>+/+</sup> mice display a  
11 reduction in fractional shortening at eight and twelve weeks compared to control  
12 littermates post TAC surgery (Con and AnkBp.E1458G<sup>+/+</sup>, N=5-6). Repeated  
13 measures two-way ANOVA mixed effects model was performed (time effect:  
14 p<0.0001, F=73.01, genotype effect: p<0.05, F=5.74, time-genotype interaction  
15 effect: p<0.01, F=3.23) with Holm-Šídák multiple comparisons test represented in  
16 figure. **C-D.** AnkBp.E1458G<sup>+/+</sup> mice do not display significant changes in left  
17 ventricular internal diameter (LVID) during systole and diastole post TAC surgery  
18 compared to control littermates. Repeated measures two-way ANOVA mixed effects  
19 model was performed ((**C**) LVIDd, time effect: p<0.0001, F=12.04, genotype effect:  
20 p<0.05, F=6.94, time-genotype interaction effect: p=0.66, F=0.68, (**D**) LVIDs, time  
21 effect: p<0.0001, F=27.28, genotype effect: p<0.05, F=7.37, time-genotype  
22 interaction effect: p=0.22, F=1.44) with Holm-Šídák multiple comparisons test  
23 represented in figure. **E-G.** Masson trichrome staining and quantitative analysis in the  
24 AnkBp.E1458G<sup>+/+</sup> mice 12-weeks post TAC surgery (Con and AnkBp.E1458G<sup>+/+</sup>,  
25 N=5). Data passed Shapiro-Wilk normality test and unpaired t-test was performed.  
26 Scale bars equal 1mm. **H.** HW/TL relative to control post TAC (Con, N=3 and  
27  
28  
29  
30  
31  
32  
33  
34  
35  
36  
37  
38  
39  
40  
41  
42  
43  
44  
45  
46  
47  
48  
49  
50  
51  
52  
53  
54  
55  
56  
57  
58  
59  
60  
61  
62  
63  
64  
65

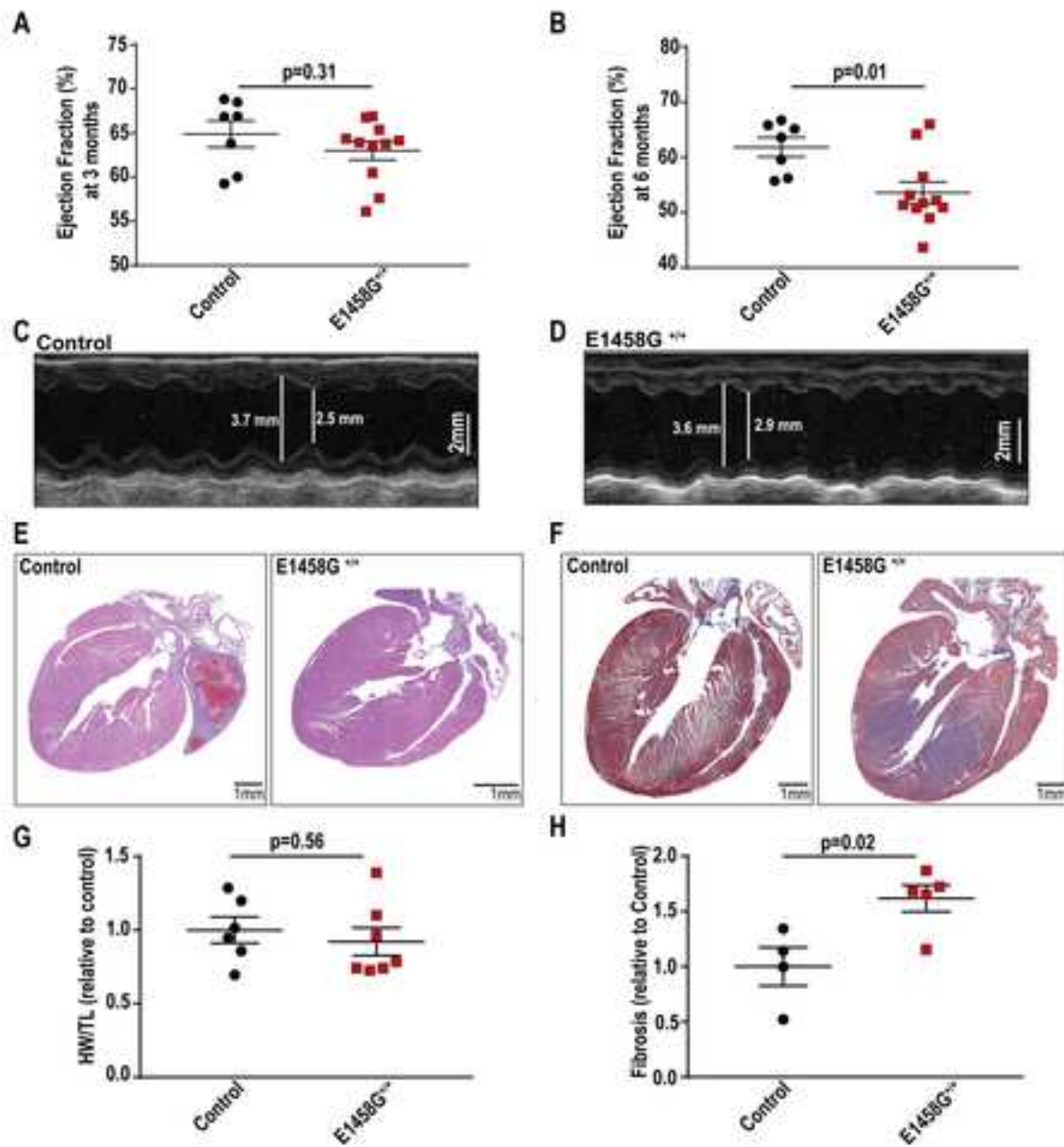
1  
2  
3  
4 AnkBp.E1458G<sup>+/+</sup>, N=5). Data passed Shapiro-Wilk normality test and unpaired t-test  
5  
6  
7 was performed. Mice were around three months at baseline before the surgery.  
8  
9

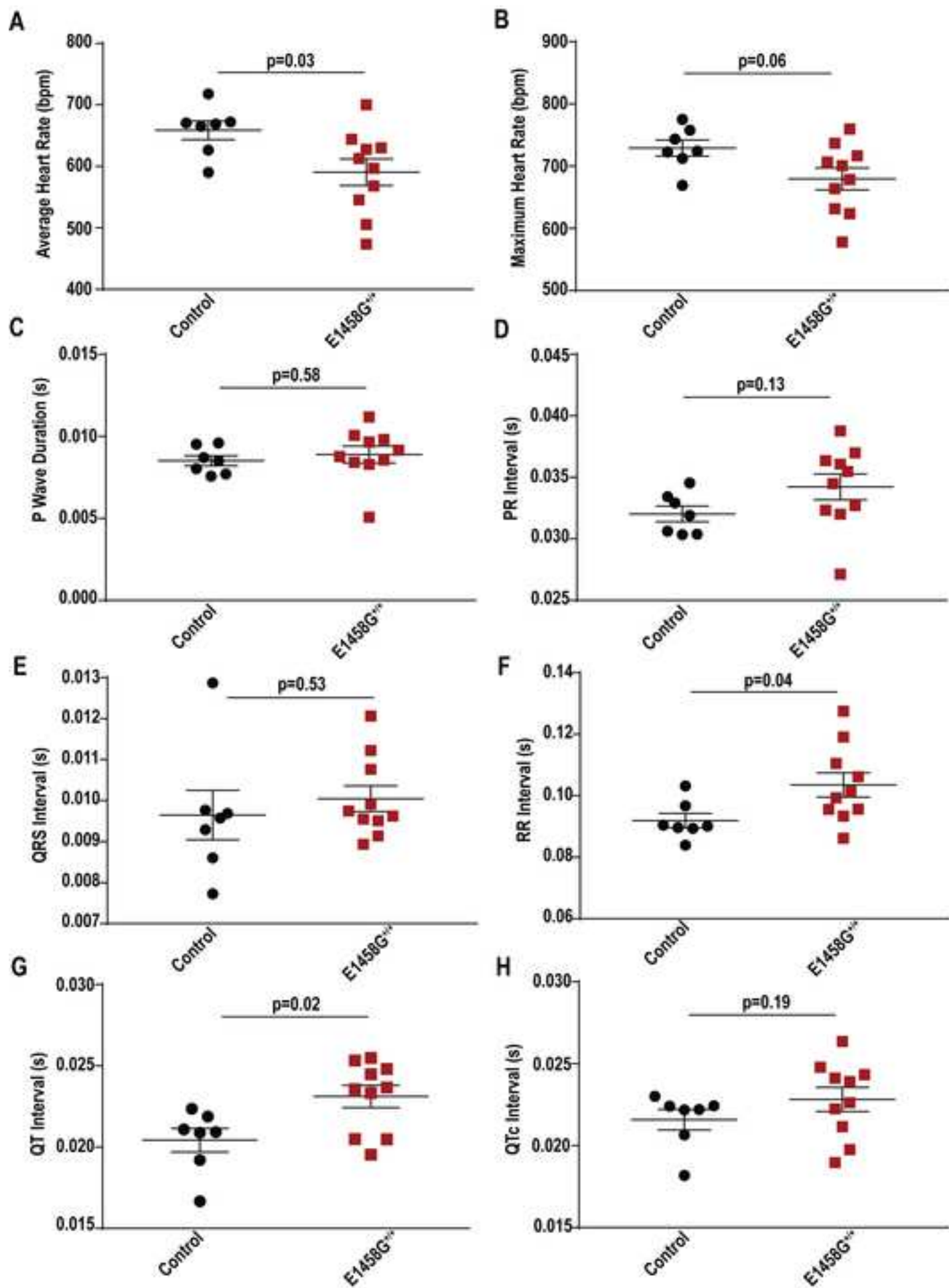
10 **Figure 9. Expression of ankyrin-B and ankyrin-binding partners in the**  
11 **AnkBp.E1458G<sup>+/+</sup> heart lysates of aged mice. A-B.** Immunoblotting and  
12 quantitative analysis of AnkB normalized to GAPDH illustrating no changes in the  
13  
14 AnkBp.E1458G<sup>+/+</sup> hearts. **C-D.** Immunoblotting and quantitative analysis of Na<sup>+</sup>/Ca<sup>2+</sup>  
15 exchanger (NCX) normalized to GAPDH showing no changes in the  
16  
17 AnkBp.E1458G<sup>+/+</sup> hearts. **E-F.** Immunoblotting and quantitative analysis of Na<sup>+</sup>, K<sup>+</sup>-  
18 ATPase (NKA) normalized to GAPDH illustrating a significant reduction in the  
19  
20 AnkBp.E1458G<sup>+/+</sup> hearts around six months of age. **G.** No significant changes in the  
21  
22 expression of AnkG normalized to GAPDH in the AnkBp.E1458G<sup>+/+</sup> hearts (Con and  
23  
24 AnkBp.E1458G<sup>+/+</sup>, N=4). All data passed Shapiro-Wilk normality tests and unpaired  
25  
26 t-tests were performed.  
27  
28  
29  
30  
31  
32  
33  
34  
35  
36

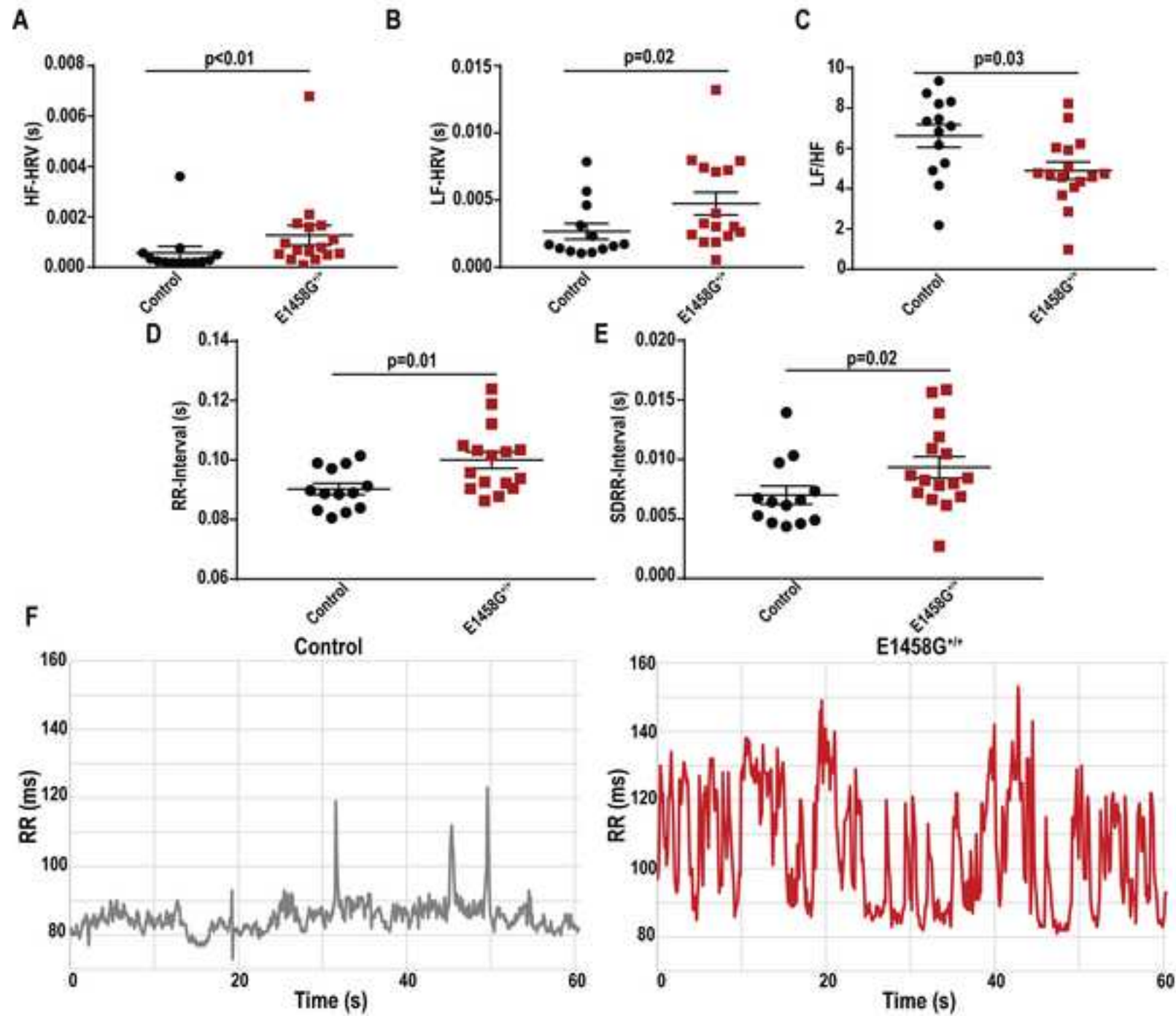
37 **Figure 10. Expression and localization of AnkB and AnkB membrane partners**  
38 **in the control and AnkBp.E1458G<sup>+/+</sup> ventricular myocytes. A.** Na<sup>+</sup>, K<sup>+</sup>-ATPase  
39 (NKA) is localized similarly in the ventricular myocytes isolated from the  
40  
41 AnkBp.E1458G<sup>+/+</sup> hearts and control hearts at ~2-3 months of age (Con, N=3; n=23  
42  
43 and AnkBp.E1458G<sup>+/+</sup>, N=3; n=21). **B.** Sodium calcium exchanger (NCX) is localized  
44  
45 similarly in the AnkBp.E1458G<sup>+/+</sup> and control ventricular myocytes at ~2-3 months of  
46  
47 age (Con, N=3; n=17 and AnkBp.E1458G<sup>+/+</sup>, N=3; n=20). **C.** NKA localization is  
48  
49 diminished in AnkBp.E1458G<sup>+/+</sup> ventricular myocytes in reference to AnkB at ~6  
50  
51 months of age (Con, N=4; n=29 and AnkBp.E1458G<sup>+/+</sup>, N=5; n=36). **D.** NCX  
52  
53 localization remains similar at ~6 months of age in AnkBp.E1458G<sup>+/+</sup> and control  
54  
55  
56  
57  
58  
59  
60  
61  
62  
63  
64  
65

1  
2  
3  
4 ventricular myocytes (Con, N=5; n=41 and AnkBp.E1458G<sup>+/+</sup>, N=5; n=38).  
5  
6 Quantitative analysis of immunofluorescence density overlap normalized to control  
7  
8  
9 (E) NKA in reference to AnkB and (F) NCX in reference to AnkB in ~2-3 months-of-  
10  
11 age mice. Quantitative analysis of immunofluorescence density overlap normalized  
12  
13 to control (G) NKA in reference to AnkB and (H) NCX in reference to AnkB in ~6  
14  
15 months-of-age mice. Data passed Shapiro-Wilk normality tests and unpaired t-tests  
16  
17 were performed (E, F and H). Data did not pass Shapiro-Wilk normality tests and  
18  
19 non-parametric (Mann-Whitney test) was performed (G). Scale bars equal 20µm.  
20  
21  
22  
23  
24  
25  
26  
27  
28  
29  
30  
31  
32  
33  
34  
35  
36  
37  
38  
39  
40  
41  
42  
43  
44  
45  
46  
47  
48  
49  
50  
51  
52  
53  
54  
55  
56  
57  
58  
59  
60  
61  
62  
63  
64  
65

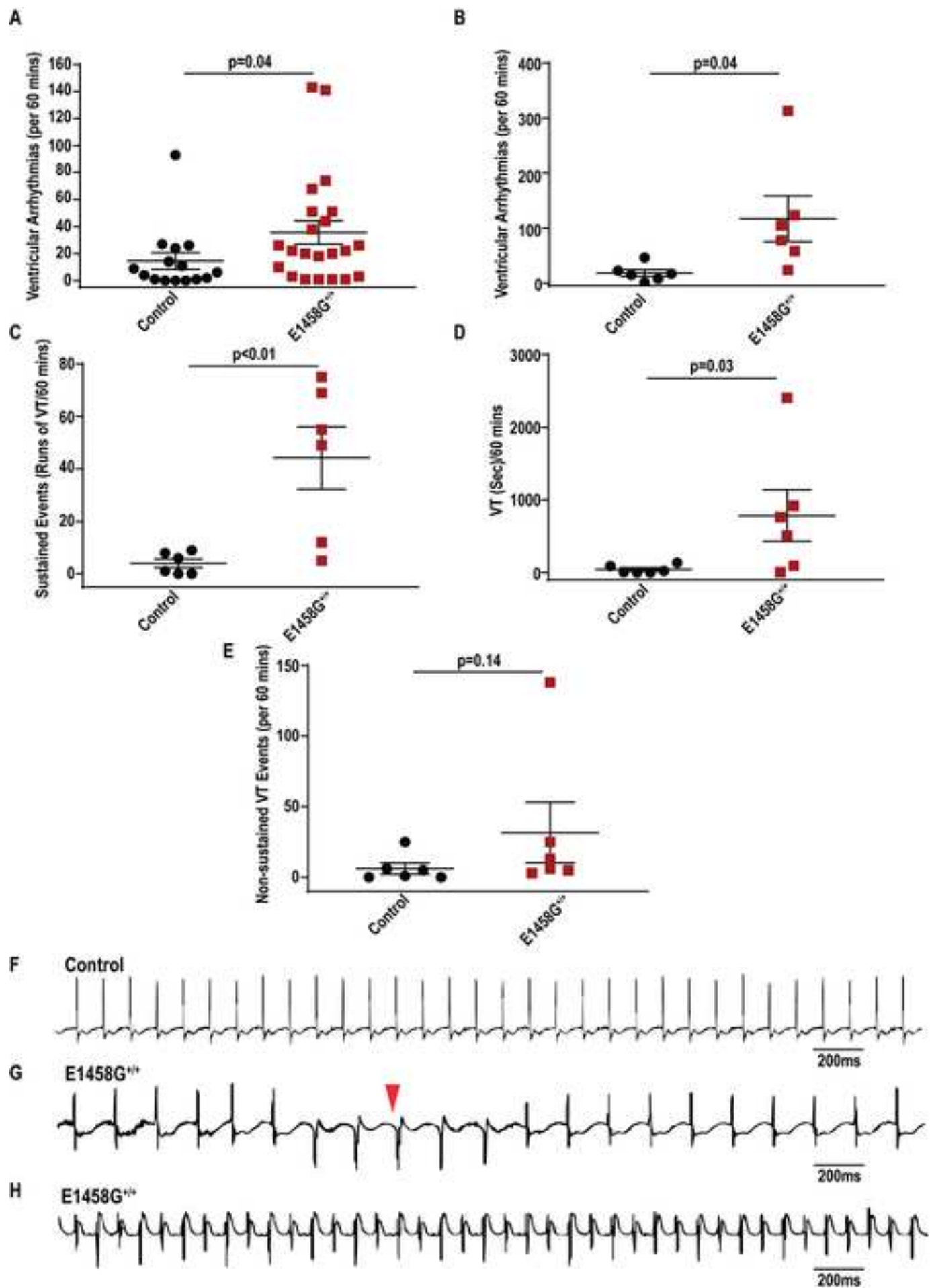


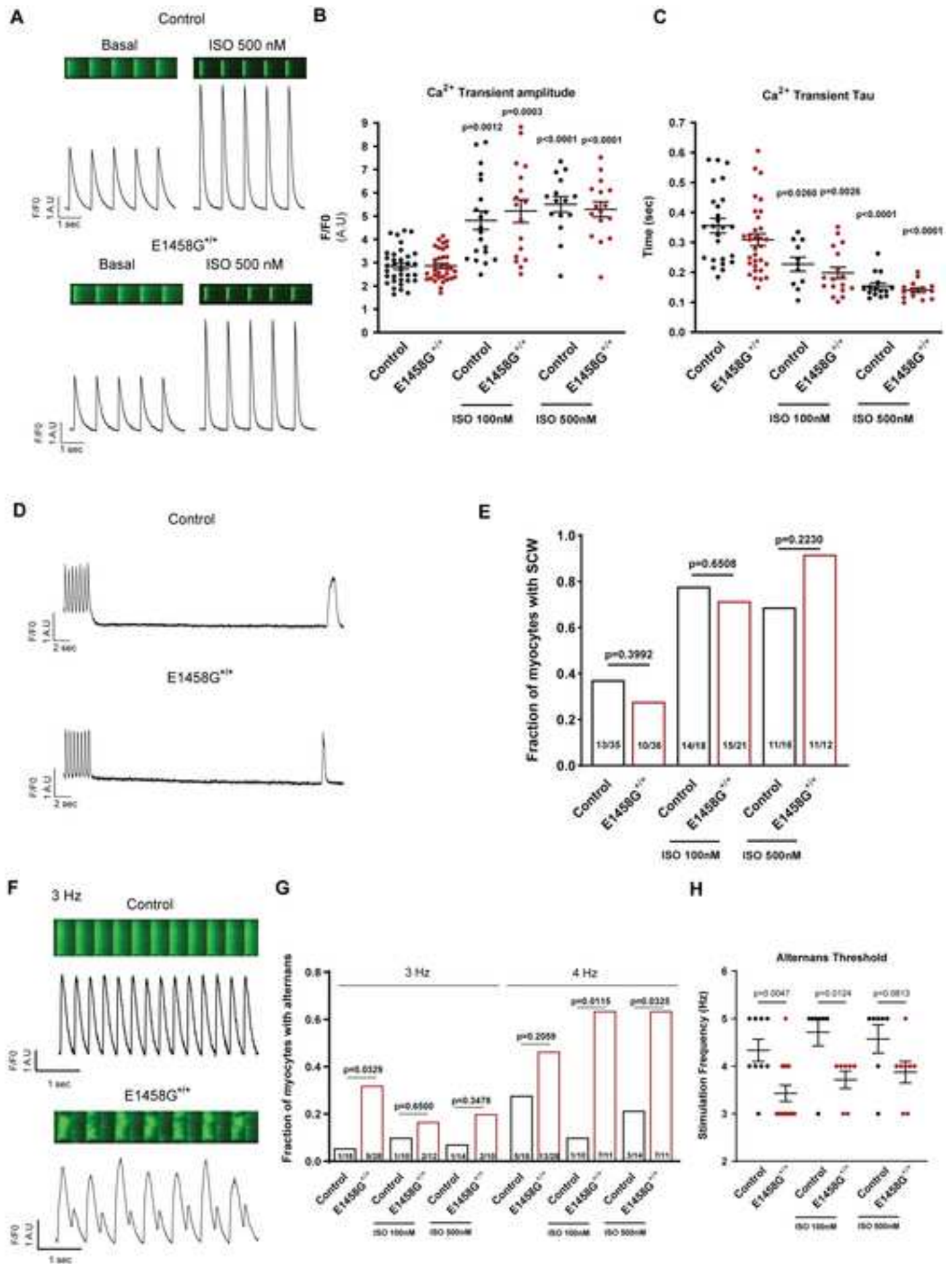


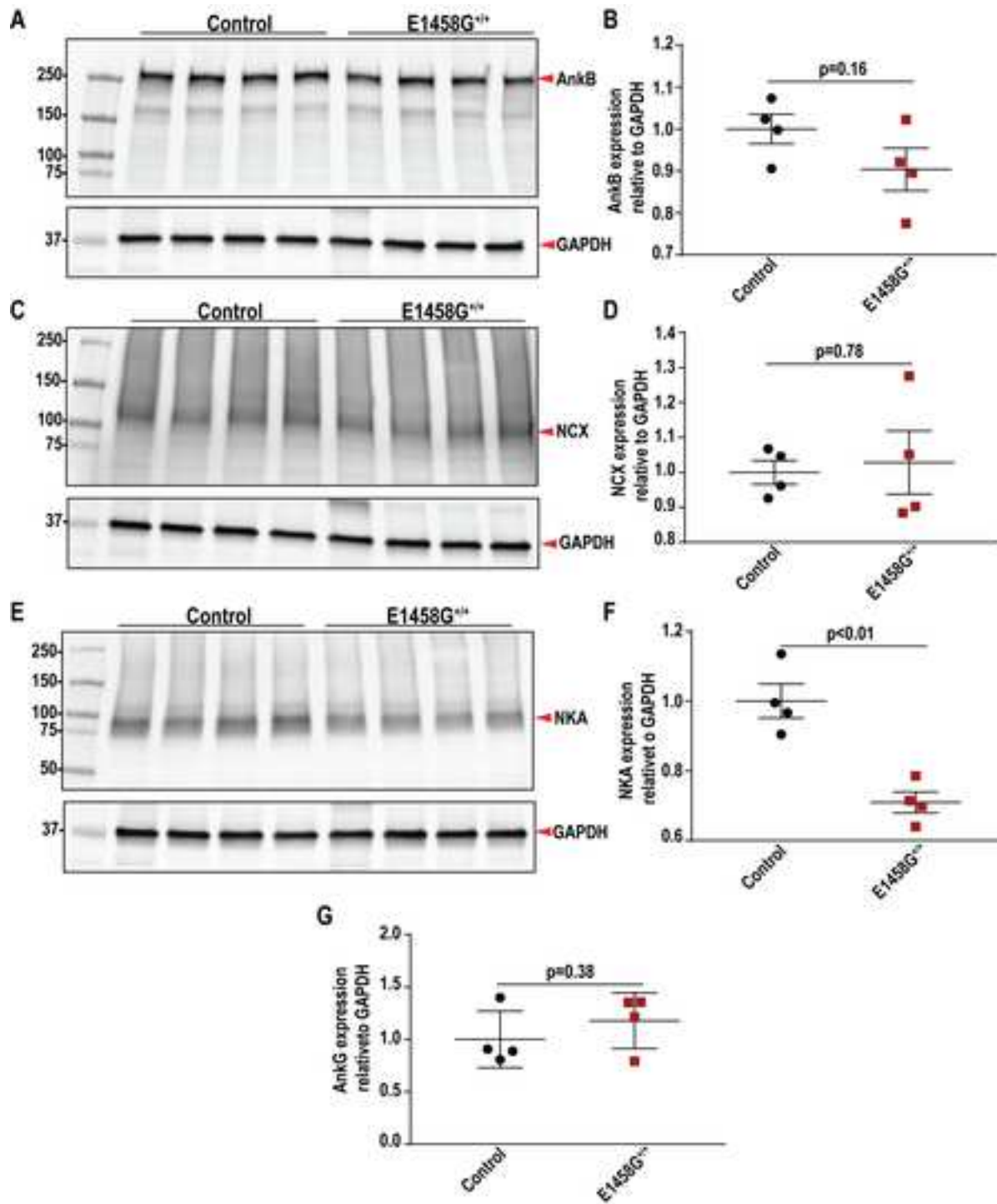


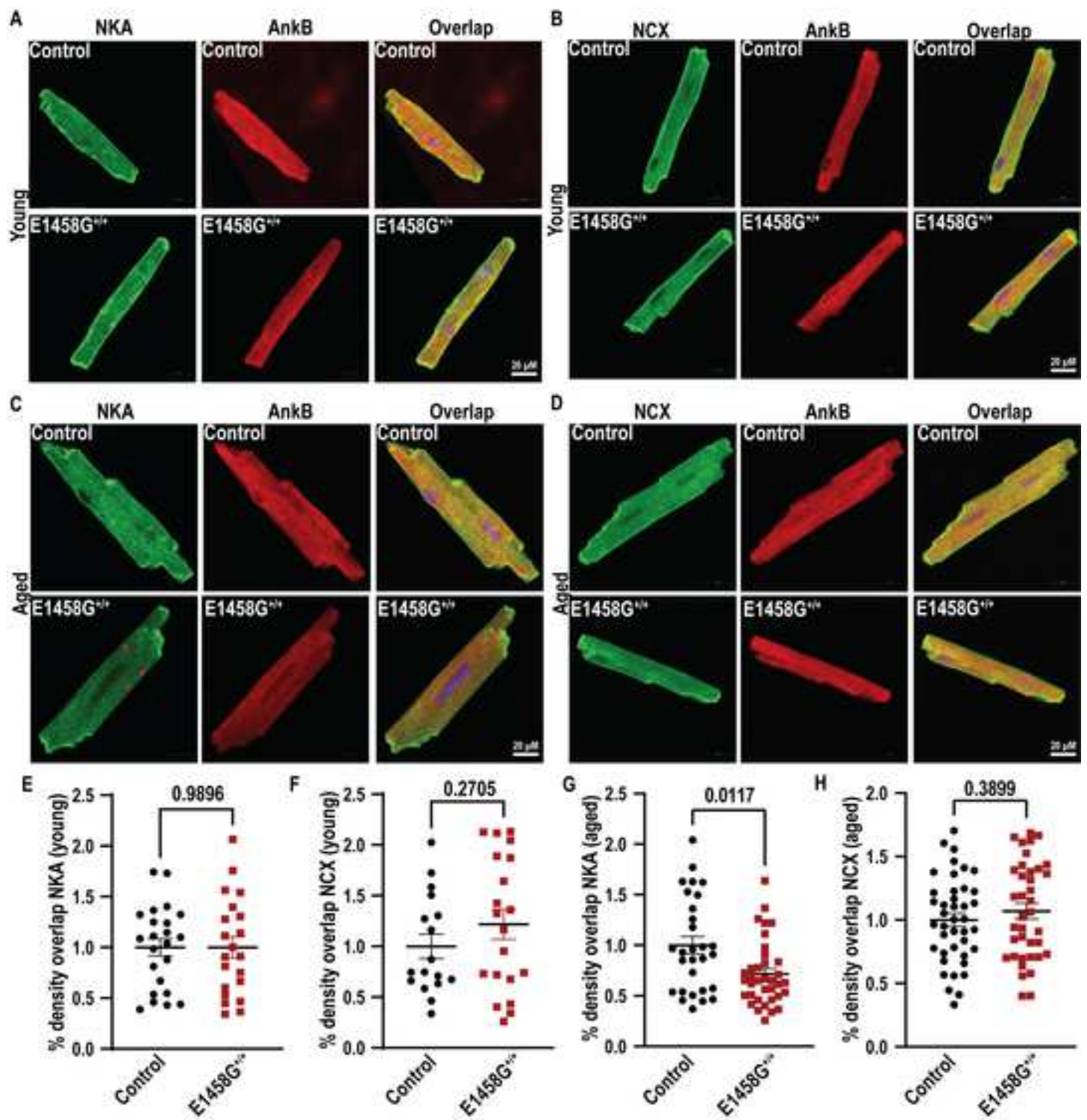


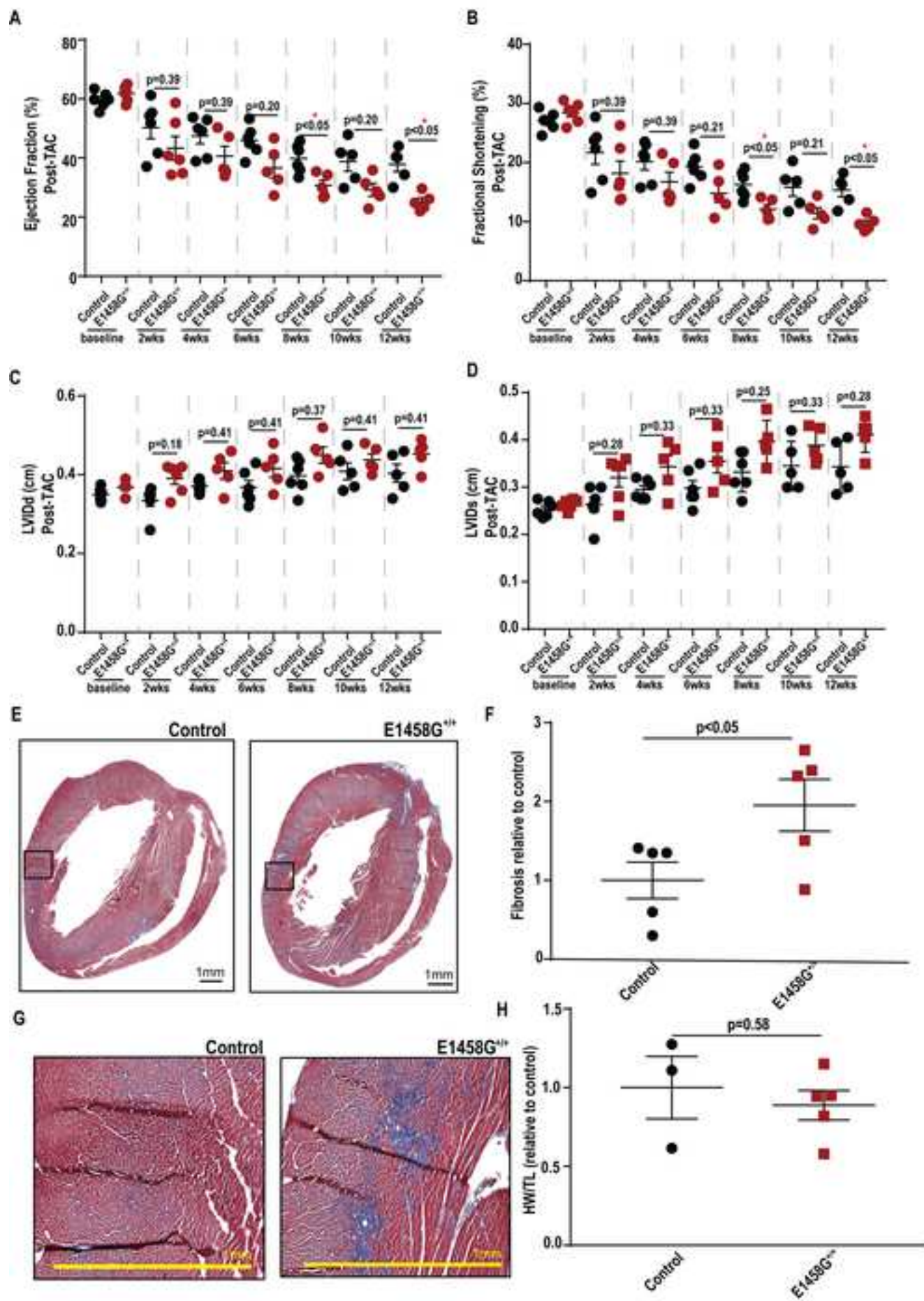










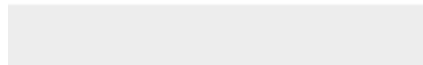
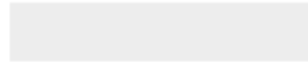




[Click here to access/download](#)

**Supporting Information (For Publication)**

Supporting Informan April 10 No track changes.docx



**Michael J. Wallace:** Methodology, Software, Validation, Formal analysis, Investigation, Data Curation, Writing-Original Draft, Writing - Review & Editing, Visualization

**Nipun Malhotra:** Investigation, Methodology, Software, Formal Analysis, Data Curation, Writing - Review & Editing

**Juan Ignacio Elio Mariángelo:** Investigation, Methodology, Software, Formal Analysis, Data Curation, Writing - Review & Editing

**Tyler L. Stevens:** Methodology, Software, Validation, Investigation, Data Curation, Writing - Review & Editing

**Lindsay J. Young:** Methodology, Software, Validation, Investigation, Data Curation, Writing - Review & Editing

**Steve Antwi-Boasiako:** Methodology, Software, Validation, Investigation, Data Curation, Writing - Review & Editing

**Danielle Abdallah:** Investigation, Data Curation, Writing - Review & Editing

**Sarah Sumie Takenaka:** Investigation, Data Curation, Writing - Review & Editing

**Omer Cavus:** Investigation, Data Curation, Writing - Review & Editing

**Nathaniel P. Murphy:** Methodology, Writing - Review & Editing

**Mei Han:** Investigation, Writing - Review & Editing

**Xianyao Xu:** Investigation, Writing - Review & Editing

**Matteo E. Mangoni:** Methodology, Data Curation, Writing - Review & Editing, Funding Acquisition

**Thomas J. Hund:** Data Curation, Writing - Review & Editing, Funding Acquisition

**Jason D. Roberts:** Methodology, Data Curation, Writing-Original Draft, Writing - Review & Editing, Visualization

**Sandor Györke:** Methodology, Data Curation, Formal analysis, Writing - Review & Editing, Visualization

**Peter J. Mohler:** Conceptualization, Supervision, Project administration, Funding acquisition, Writing-Original Draft, Writing - Review & Editing, Visualization

**Mona El Refaey:** Conceptualization, Supervision, Project administration, Methodology, Formal analysis, Data Curation, Writing-Original Draft, Writing - Review & Editing, Visualization

[Click here to view linked References](#)



[Click here to access/download](#)

**Revised Manuscript (with tracked changes)**  
E1458G May 2023.docx

